Bachelor-Arbeit
Geowissenschaften

High-pressure modifications of silicon

vorgelegt von
Jannik Richter
aus Kirchheim/Teck

BetreuerInnen
Dr. A. Danilewsky
Prof. Dr. A. Cröll

Freiburg, den 23.06.2013

TABLE OF CONTENTS

1 ABSTRACT

For the investigation of high-pressure modifications of silicon in this thesis, dynamic measurements were performed using powder diffraction with a diamond anvil cell at DESY. Different samples at different pressure gradients were measured and analyzed using the Rietveld method.

The following phase transformations are observed with increasing pressure:

$$Si\ I \rightarrow Si\ II \rightarrow Si\ XI \rightarrow Si\ V \rightarrow Si\ VI$$

The pressure ranges of the individual phases are shifted to lower pressures at higher pressure gradients. Analog, the boundaries of the pressure ranges of the phases Si XI, Si V and Si VI are shifted to lower pressures at pressure relief. By comparison with the literature, it was shown that the pressure regions at static and dynamic conditions are pretty similar, whereas at dynamic conditions they are slightly shifted to higher pressures. Only the phase Si II has a strongly limited pressure range at dynamic conditions. Furthermore, the lattice parameters of the individual phases at the different pressure conditions could have been refined by the Rietveld method. Within the inaccuracy the lattice parameters are consistent with the literature values. For the until now little described phase Si VI, the lattice parameters could have been refined in dependence of the pressure.

2 INTRODUCTION

Silicon represents one of the most important semiconductors in today's high-performance electronics (Hull, 2005). By the processing in the industry locally high pressures, which lead to phase transitions, emerge during the mechanical treatment and the wafer handling. This can lead to a change of the electronic properties of the material, as well as the formation of cracks and the breaking of the wafers (Jang *et al.*, 2003). Of the currently known 13 modifications of silicon (Hull, 2005), some transform from other phases by pressure relief (Hu *et al.*, 1986).

The aim of this thesis is to investigate the high-pressure modifications of silicon at dynamic conditions in disequilibrium using powder diffraction in a diamond anvil cell at the DESY Hamburg.

The thesis is structured as follows:

To give the reader a quick introduction, chapter 1 summarizes the entire thesis including the most important results. Subsequently the theoretical background is given in Chapter 3, explaining the theory of phases, X-ray powder diffraction, synchrotron radiation and the analysis using the Rietveld refinement. Chapter 4 gives an introduction to the high-pressure modifications of silicon, relevant for this work. In Chapter 5, the experimental setup, the sample preparation, the execution of the experiments and the programs and parameters used for the analysis are described. This is followed by the results of the individual analyzed measurements, which then are discussed in chapter 7. In the final chapter 8, the references cited in this work are listed.

3 THEORY

3.1 X-ray diffraction

X-ray diffraction (XRD) is a method for qualitative and quantitative analysis of crystalline samples. In this method the interaction of X-rays and the lattice of a crystal is used. Since X-rays and the lattice parameters of crystals have the same magnitude, the radiation is diffracted. The elastically diffracted portion of the radiation leads to structural characteristic intensity maxima, whereas inelastic collisions lead to emission of a continuous background radiation (Spieß *et al.*, 2009).

Bragg's law

1912 W. L. Bragg introduced an equation to describe X-ray diffraction by crystals. The diffraction is described as selective reflection on a set of lattice planes. This means, if monochromatic X-rays of the wavelength λ hit a set of lattice planes (hkl) with the lattice plane spacing d_{hkl}, then, at a distinct angle Θ_{hkl} between the incident beam and the set of lattice planes, it leads to partial reflection. This angle Θ_{hkl} is called Bragg or grazing angle. The high-energy X-rays also penetrate deeper into the crystal, where they get reflected the same way at a subjacent lattice plane of the same set of lattice planes (Spieß *et al.*, 2009).

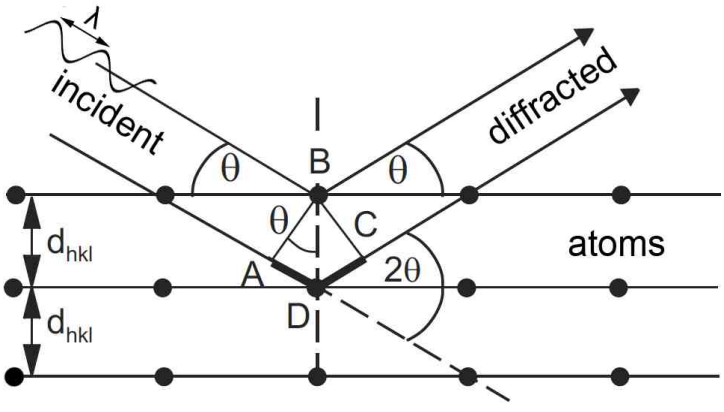

***Figure 3.1**: reflection of X-rays on a set of lattice planes (Spieß et al., 2009)*

As seen in figure XX, the deeper penetrating beam covers a distance, which is longer by $\overline{ADC}$. As a function of the wavelength λ and the diffraction order n, this length is defined as:

$$\overline{ADC} = n \cdot \lambda \qquad \text{Eq. 3.1}$$

Is this length an integer multiple of the wavelength, it results in constructive interference. The relation between the Bragg angle Θ_{hkl}, the lattice plane spacing d_{hkl} and the wavelength λ, is described by the Bragg's equation (Spieß *et al.*, 2009):

$$n \cdot \lambda = 2 \cdot d_{hkl} \cdot \sin \theta_{hkl} \qquad \text{Eq. 3.2}$$

By measuring a sample in a 2Θ-region an intensity distribution of the diffracted X-ray radiation, a so-called diffraction pattern, is recorded. The maxima of intensity are called peaks and can be described by profile functions such as Gaussian or Lorentz distribution. The measured underground is especially sensitive in the flanks of the peaks. Therefore the full width half maximum (FWHM) is used for the analysis of diffraction patterns (Spieß *et al.*, 2009).

For the X-ray diffraction of this thesis powder samples are used. The orientations of the crystals in the powder are statistically distributed, whereby all reflections can be measured simultaneously. This would not be possible with a monochromatic single crystal image. By recording with an area detector, rings, as in the Debye-Scherer camera, are recorded. These get converted into diffraction patterns by integration (Spieß *et al.*, 2009). In a diffraction pattern, the peak locations describe the metric of the unit cell, whereas the position of the atoms is determined by the intensities of the peaks (Borchardt-Ott, 2009).

3.2 Analytical methods

In preparation for the analysis, correction models such as for underground radiation are often applied to the diffraction patterns. For the analysis of the recorded diffraction patterns different qualitative and quantitative methods, as well as methods for crystal structure analysis or refinement of crystal structures, are available. By mathematical description of the individual peaks, as well as the whole diffraction patterns, information about peak positions and intensity ratios is obtained and analyzed. Currently the Rietveld refinement, which was originally developed for

crystal structure analysis, is the most important analytical method (Spieß *et al.*, 2009).

The Rietveld refinement, which can be used for all the analyses mentioned above, uses the method of least squares to fit analytical functions to the measured diffraction pattern. For the Rietveld refinement structural models of the relevant phases are needed (Spieß *et al.*, 2009).

For further information refer to Spieß et al (2009): “Moderne Röntgenbeugung”.

3.3 Phase transitions

A phase denotes a particular state of a substance system, which is defined by the thermodynamic state variables. Pressure, temperature and chemical composition represent the independent state variables. By the application of pressure, the crystal lattice is deformed, leading to a phase transition. Displacive and reconstructive transitions are differentiated (Kleber *et al.*, 2010).

3.4 Synchrotron radiation

In a synchrotron radiation source, electrons are accelerated and held on a circular orbit by magnets. By the deviation of the electrons electromagnetic radiation is emitted which can be used to carry out experiments. Compared with laboratory X-rays, the emitted radiation has a high intensity, a strong focus and a defined wavelength (Wille, 1996).

For further information refer to Wille, K. (1996): “Physik der Teilchenbeschleuniger und Synchrotronstrahlungsquellen: Eine Einführung”.

4 STRUCTURES

Currently 13 modifications of silicon are known, which result from different pressure, temperature and unloading. The stable phase at normal conditions is Si I with a cubic diamond structure in the space group $Fd\bar{3}m$ (Katzke *et al.*, 2006). In the experiments high-pressure modifications, starting from Si I, has been measured by dynamic pressure changes. The structural parameters of the

modifications relevant for this work are listed in the following table 4.1.

***Table 4.1**: overview of the structural parameters of the modifications of silicon relevant for this work*

Modification	Space group	Structure	Lattice parameters [Å]	Pressure region [GPa]	Reference
Si I	$Fd\bar{3}m$	Cubic diamond structure	a = 5.43	0 - 12	(Dutta, 1962), (Katzke *et al.*, 2006)
Si II	$I4_1/amd$	β-Sn	a = 4.69 c = 2.58	8.8 - 16	(Hu & Spain, 1984)
Si V	P6/mmm	Primitive hexagonal	a = 2.53 c = 2.37	14 - 35	(Olijnyk *et al.*, 1984)
Si VI	Cmca	x = 0.218 (8d) y = 0.328 (8f) z = 0.173 (8f)	a = 7.97 b = 4.78 c = 4.75	34 - 40	(Hanfland *et al.*, 1999)
Si XI	Imma	Body centered orthorhombic	a = 4.74 b = 4.50 c = 2.55	13 - 15	(McMahon & Nelmes, 1993)

At pressure build-up silicon transforms as follows (Hull, 2005):

$$Si\ I \rightarrow Si\ II \rightarrow Si\ XI \rightarrow Si\ V \rightarrow Si\ VI$$

The phase transitions are displacive transformations without sharp boundaries (Katzke *et al.*, 2006). Multiphase fields are observed over wide pressure ranges (Hu & Spain, 1984). In figure 4.1, the cubic diamond structure of Si I is shown.

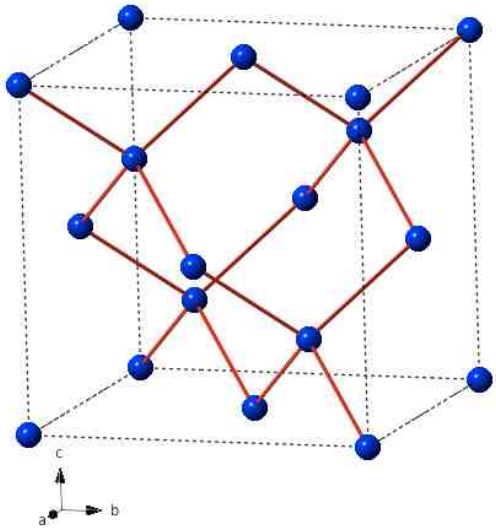

***Figure 4.1**: unit cell of Si I, $Fd\bar{3}m$, cubic diamond structure, the orientation of the unit cell is shown bellow (created with CrystalMaker 8.5)*

In the transformation from Si I to Si II, which is shown in figure 4.2, the cubic diamond structure is stretched along the [100]- and [010]-direction, while the [001]-direction is drastically shortened. Thereby the atoms migrate from the 8a to the 4a Wyckoff positions, which leads to a change in the coordination number from 4 to 6. In this phase transition from the cubic to the tetragonal crystal system, a decrease in volume of ~23.7% occurs between normal conditions and 12-13 GPa (Katzke *et al.*, 2006).

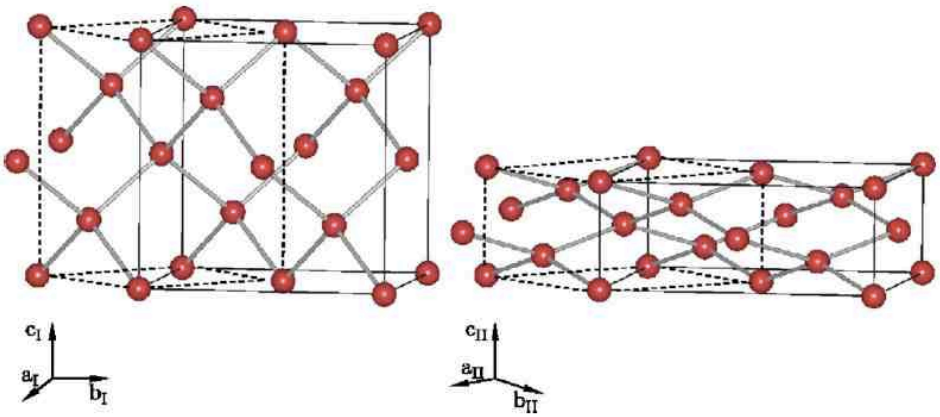

***Figure 4.2**: phase transition from Si I (left) to Si II (right), the orientations of the unit cells are shown bellow (Katzke et al., 2006)*

The ß-Sn structure resulting from this phase transition is shown in figure 4.3.

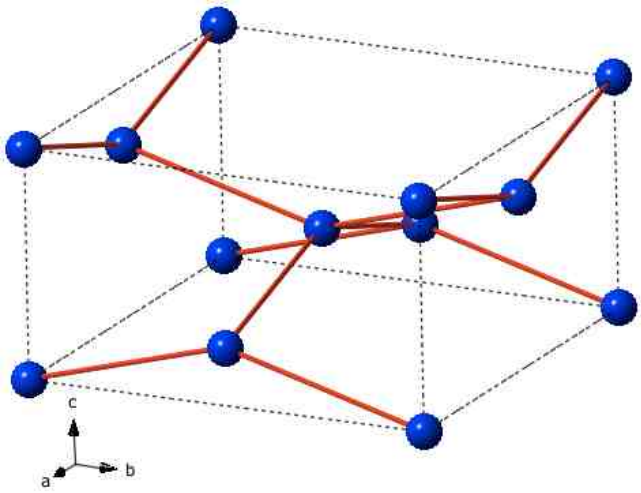

***Figure 4.3**: unit cell of Si II, $I4_1/amd$, ß-Sn structure, the orientation of the unit cell is shown bellow (created with CrystalMaker 8.5)*

By antiparallel displacement of the atoms along the [001]-direction by ±0.068 c, the ß-Sn structure is transformed into the body centered orthorhombic structure of Si XI. Thereby the atoms migrate from the 4a to the 4e Wyckoff positions, resulting in a decrease in volume of ~0.2% (Katzke *et al.*, 2006). This transformation is shown in figure 4.4. The arrows on the atoms mark the direction of displacement.

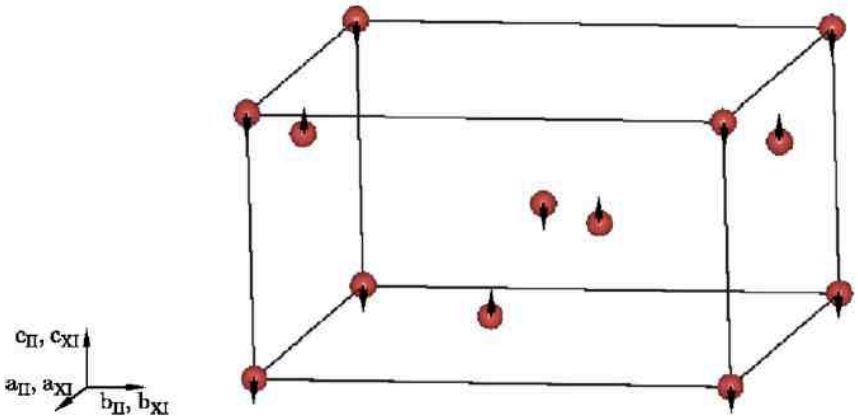

***Figure 4.4**: phase transition from Si II to Si XI, the arrows on the atoms mark the direction of displacement, the orientation of the unit cell is shown besides (Katzke et al., 2006)*

The transformation from Si XI to Si V proceeds by another antiparallel displacement of the atoms along the [001]-direction by ±0.057 c. By filling of the hexagonal 1a Wyckoff positions, the body centered orthorhombic structure transforms into the primitive hexagonal structure. This leads to a further decrease in volume of ~ 0.5%. The phase transition is shown in figure 4.5. The arrows on the atoms mark the direction of displacement (Katzke *et al.*, 2006).

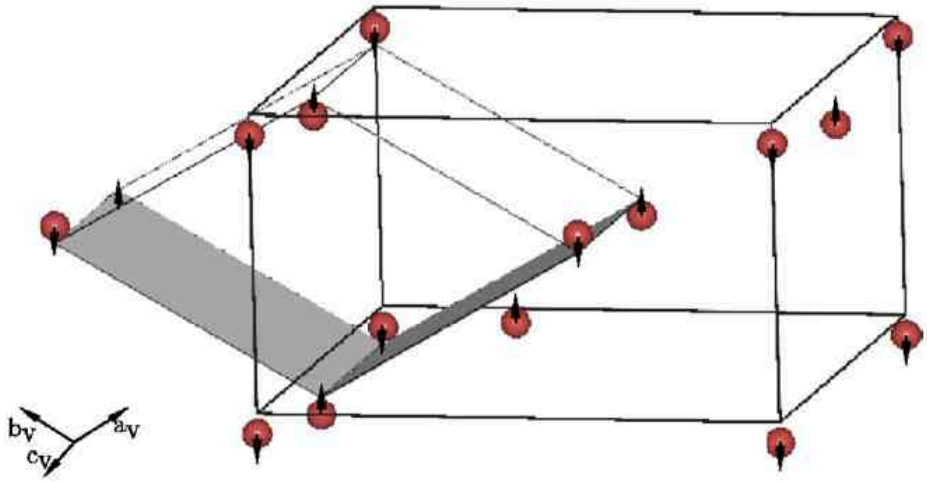

***Figure 4.5**: phase transition from Si XI to Si V, the arrows on the atoms mark the direction of displacement, the orientation of the unit cell of Si V is shown besides (Katzke et al., 2006)*

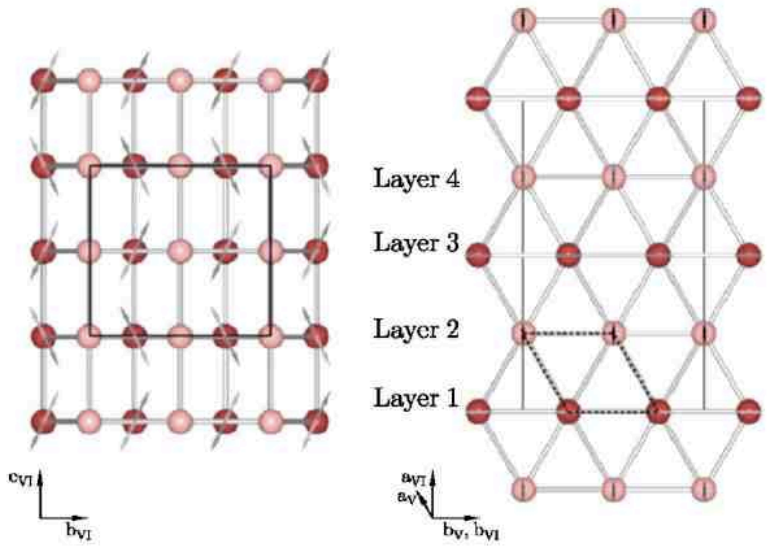

***Figure 4.6**: phase transition from Si V to Si VI, the arrows on the atoms mark the direction of displacement, the orientations of the unit cells are shown bellow (Katzke et al., 2006)*

The complex phase transition from Si V to Si VI is shown in figure 4.6. The arrows on the atoms mark the direction of displacement. The atoms of the layers 1 and 3 move in the orthorhombic b/c-plane and take the 8f Wyckoff positions with a coordination number of 11, which is shown left in figure 4.6. The atoms in the layers 2 and 4 move along the [100]-direction, taking the 8d Wyckoff positions with a coordination number of 10 (Katzke *et al.*, 2006). In figure 4.7 Si VI is shown, projected along [100] (left) and [001] (right).

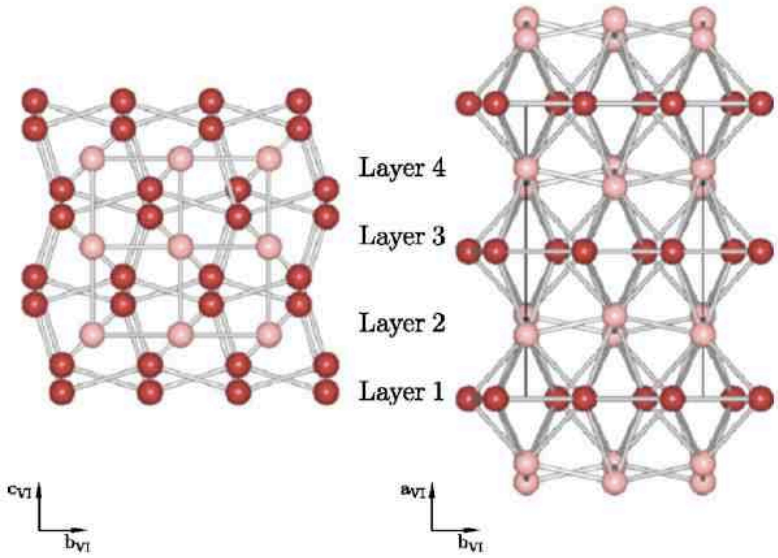

***Figure 4.7**: Si VI projected along [100] (left) and [001] (right), Cmca, special form, the orientations of the unit cells are shown bellow (Katzke et al., 2006)*

4.1 Pressure calibration

By the application of pressure on a crystalline phase, the spatial extend of the unit cell changes. In a diffraction pattern, the increase in pressure can be seen by a shift of the peaks to higher 2Θ-values. The lattice parameters of the phase can be determined using the refinement method, which then can be used to calculate the volume of the unit cell. Using the Young's modulus the volume is used to calculate the actual pressure (Anderson *et al.*, 1989).

For the pressure calibration of the diamond anvil cell in the experiments, some gold was added to the Si-samples in the sample carrier. In the considered pressure- and temperature-range of the

experiments no phase transition of gold takes place. Therefor gold is more suitable for the pressure calibration than for example NaCl. The equation of state, as described in detail in Anderson et al, can be written in a general form as a function of pressure *P*, volume *V* and temperature *T* as follows (Anderson *et al.*, 1989):

$$P(V,T) = P(V,0) + P_{TH}(V,T) \qquad \textbf{Eq. 4.1}$$

The second term on the right side of equation 4.1 describes the thermal pressure (Anderson *et al.*, 1989). Since the measurements were performed at a constant temperature, it is neglectable. By applying the Birch-Murnaghan equation of state (Birch, 1952) for the first term on the right side of equation 4.1 we obtain:

$$P(V,T) = \frac{3}{2}K_{T_0}\left[\left(\frac{V_0}{V}\right)^{\frac{7}{3}} - \left(\frac{V_0}{V}\right)^{\frac{5}{3}}\right]\left[1 - \varepsilon\left\{\left(\frac{V_0}{V}\right)^{\frac{2}{3}} - 1\right\}\right] \qquad \textbf{Eq. 4.2}$$

With $$\varepsilon = \frac{3}{4}[4 - (\delta K_T/\delta P)_T]$$

Where V_0 is the volume of the unit cell at normal conditions, V is the volume of the unit cell at the pressure to be determined, K_{T_0} is the Young's modulus at normal conditions and $(\delta K_T/\delta P)_T$ is the change of the Young's modulus per pressure change at a given temperature.

Since the measurements take place under normal temperature conditions, the following values for the pressure calculations are used (Anderson *et al.*, 1989):

$$K_{T_0} = 166.65\ GPa$$

$$(\delta K_T/\delta P)_T = 5.4823$$

5 EXPERIMENTS

5.1 Beamline

The measurements were performed at the Deutsches Elektronen-Synchrotron, short DESY, in Hamburg. With the Positron-Elektron-Tandem-Ring-Anlage PETRA III a highly brilliant radiation source is available, which is one of the best X-ray radiation sources in the world. The high intensity and strong focusing of the available radiation enables the recording of complete diffraction patterns in seconds. For the study of dynamic phenomena under extreme pressure and temperature conditions using X-ray diffraction the Extreme Conditions Beamline (ECB) P02.2 is set up. Onto the samples in the diamond anvil cell temperatures of 25 - 1500 K and pressures of 1 - 4 Mbar can be applied. The setup of the beamline is shown in figure 5.1.

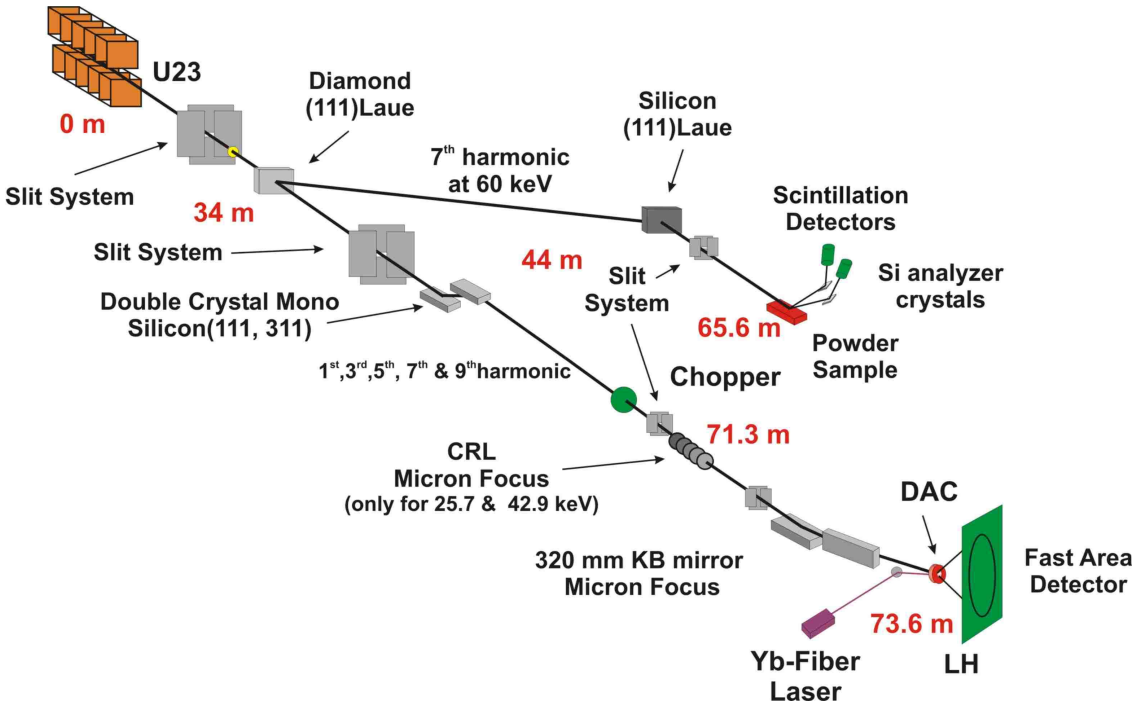

***Figure 5.1**: schematic illustration of the setup of the Extreme Conditions Beamline ECB P02.2*

The beamline is divided in an Optics Hutch (OH) and an Experimental Hutch (EH). After the emission of the radiation at the 2 m long undulator U23, the beam is directed into the optics hutch,

where it is monochromatized and focused by monochromators, mirrors etc. Thus a highly focused beam with a diameter of 1 - 2 µm and a high intensity is achieved. For the measurements a wavelength of 0.28988 Å was present. The experimental setup is located in the experimental hutch. The beam is directed onto the sample in the adjustable diamond anvil cell, which is mounted on a tripod. The beam is diffracted according to Bragg's law and measured with a Perkin Elmer XRD 1621 area detector. This has an area of 400 x 400 mm^2 with 2048 x 2048 pixels and a maximum counting rate of 63000 counts/sec. The exposure time depends on the sample and is between 1 - 8 sec. For the pressure build-up a He-membrane is attached to the diamond anvil cell and put into the membrane box. The setup of the ECB provides optimal conditions for the performance of dynamic experiments with silicon under extreme pressure and temperature conditions. The setup allows non-hydrostatic and hydrostatic measurements at pressure build-up and relief. Figure 5.2 shows a schematic illustration of the diamond anvil cell with the He-membrane in the installed state.

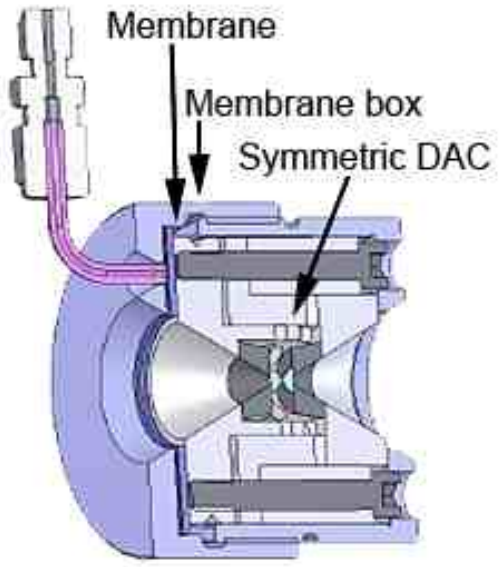

***Figure 5.2**: schematic illustration of the diamond anvil cell with the He-membrane and the membrane box*

5.2 Samples

***Table 5.1**: overview of the samples used in the experiments*

Sample	Lattice parameter [Å]	Korngröße	Source
Si-standard	a = 5.43159 ± 0.00020	1 - 10 µm (90%< 6.76)	National Institute of Standards and Technology SRM 640d
Si-wafer	a = 5.4154392 ± 0.0014976	-	handpowdered Si:B-wafer
Si-nanopowder	a = 5.4154392 ± 0.0014976	40 - 80 nm (Ø = 60nm)	Ionic Liquids Technologies GmbH, Silicon nanopowder

The evaluated experiments of this thesis were all measured with the sample Si-standard, which is highlighted in gray in table 5.1. The lattice parameters of the samples Si-wafer and Si-nanopowder were obtained by a Rietveld refinement of run02 and run06 in the program TOPAS. In the diffraction patterns of both samples an unidentified peak occurs at 23.23° 2Θ.

5.3 Loading of the diamond anvil cell

For the preparation of the sample carriers and the loading of the diamond anvil cells, a laboratory, which belongs to the beamline, is available.

Preparation of the sample carriers

A 250 µm thick rhenium plate is glued onto a steel plate with a hole in it. For this purpose, only two small splices of superglue are used to prevent contamination. After the glue has dried, a line is drawn on the steel plate to mark the orientation in the diamond anvil cell. To fill in the sample, a 100 µm sized hole must be drilled into the Re plate. For this purpose, the Re plate is initially indented. Three spring rings are inserted into the lower half of the cell, on which the steel plate, with the rhenium plate glued on, is placed. After checking the orientation, the top half of the cell is

placed on it and the Re plate is indented by tightening of the cell via the screws. The thickness of the plate should be around 35 µm (min.: 30 µm, max.: 50 µm) at the indented position. This is checked using a micrometer caliper. Then, a hole with 100 µm diameter is drilled into the center of the indentation using an arc-driller. For the centering of the bore, a microscope and two micrometer screws are used. These allow a displacement of the work table in two direction, 90° to each other. As medium turpentine substitute is used, which gets filled into the drilling shell using a pipette. After lowering the driller onto the sample carrier and programming of the drilling depth, the drilling is started. Once the drilling is completed, the sample carrier is taken out and cleaned with acetone and compressed air. It is checked, if the hole is centered and pervasive using a light microscope. Subsequently, the sample carrier can be installed and loaded in the diamond anvil cell.

Loading of the cell

Before loading the diamond anvil cell, it needs to be cleaned. For this purpose, the surfaces of the diamonds are cleaned using thin stripes of sandpaper. After exhausting of contaminants using compressed air and cleaning of the diamonds using acetone, the cell must be checked under a microscope for cleanliness and integrity. Subsequently, the cell can be loaded. In addition to the sample carrier, two or three wax spheres are put into the lower part of the cell for fixation. The upper part of the cell is attached and the orientation of the sample carrier is checked using the light microscope. If light passes through the bore, it is placed properly. After removal of the upper part, a little amount of the powder sample can be placed into the bore using a needle. By compression of the cell using the upper part, the sample is pressed in. After removal of the upper part, the sample is checked and excess powder around the bore is removed. For pressure calibration, some gold powder is added. It should be noted, that only a very little amount of gold is added. Thereupon, the upper part of the cell is cleaned and the sample is pressed in again. After a further control of the sample without the upper part using the light microscope, the cell is finally closed and screwed. In the microscope, the powder sample, as well as some gold should be visible. The

loaded cell is ready to get installed into the beam path.

Installation of the cell into the beam path

Together with the He-membrane, the diamond anvil cell is incorporated into the membrane box. It should be noted, that the He-membrane and the dark cone of the cell are mounted on the side facing away from the beam. After screwing of the membrane box, it can be fixed in the provided tripod. The tripod is then being installed in the beam path. To close the experimental hutch an interlock search needs to be performed. The sample is then ready for the measurement.

5.4 Execution of the experiment

At the beginning of the measuring time a calibration on the applied radiation needs to be performed. For the calibration the program fit2d of the European Synchrotron Radiation Facility (ESRF), which was developed by Dr. Andy Hammersley, is used. As a graphical user interface of fit2d the program GSE_shell V1.04 is used. Dr. Przemek Dera developed this program at the Argonne National Laboratory. By marking some points on the rings of the recording a calibration file is created. A screenshot of the calibration of the 09.12.2012 in the program GSE_shell V1.04 is shown in figure 5.3.

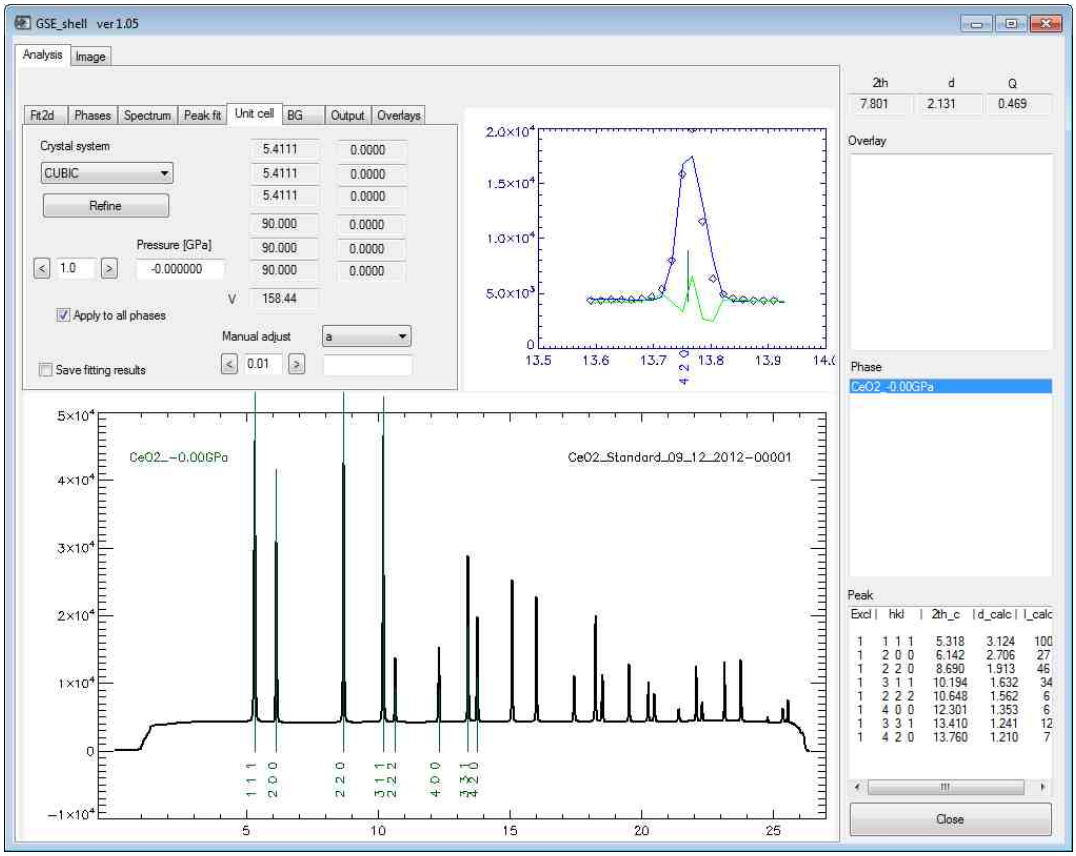

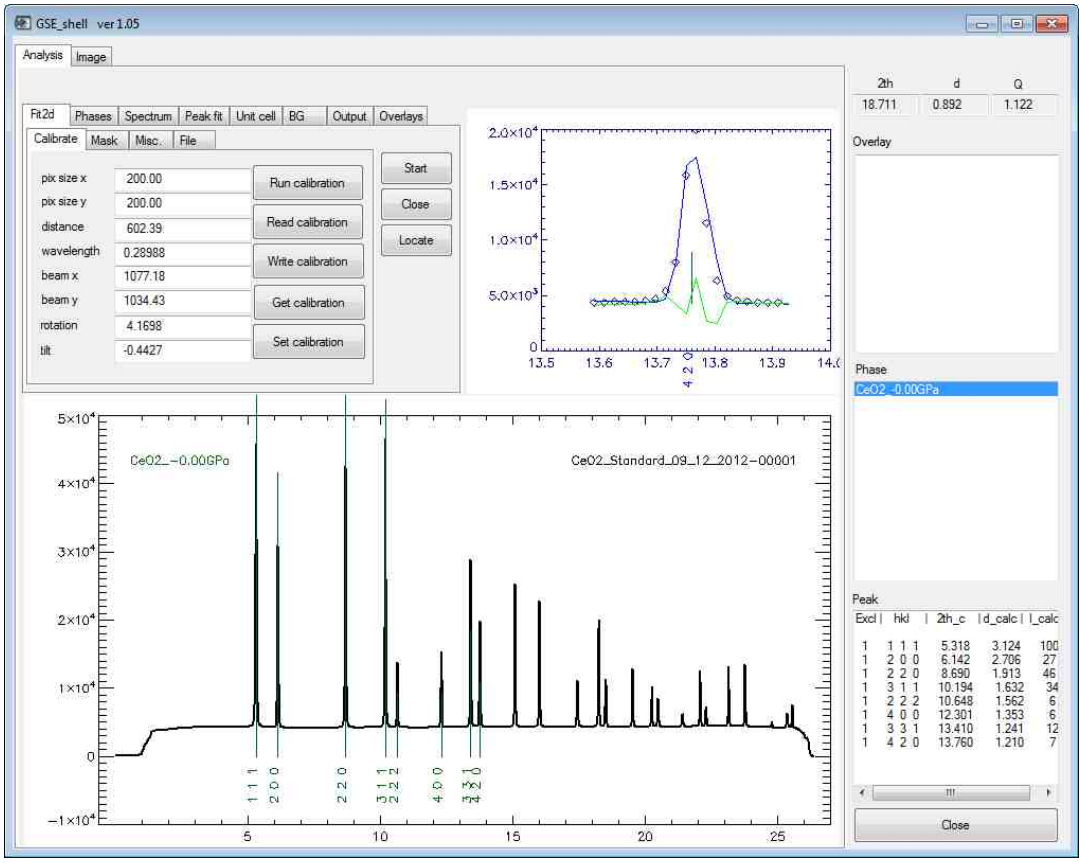

***Figure 5.3**: screenshot of the calibration of the 09.12.2012 using CeO_2 in GSE_shell V1.04*

The measurements at the ECB are controlled using computers in a room next to the experimental hutch. Before the measurements are started, the sample must be adjusted. To do this, the shutter is opened and a diode is retracted between the diamond anvil cell and the detector. This can be controlled using a camera. The cell in the tripod is centered horizontally and vertically first. For this purpose, a measurement of the absorption of the diamond anvil cell is performed. A curve, as shown in figure 5.4, results.

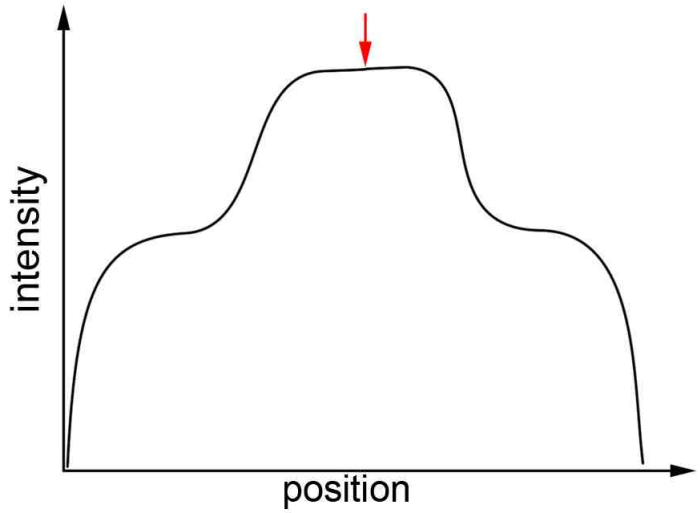

***Figure 5.4**: schematic curve shape of the measurement of the absorption of the diamond anvil cell for the horizontal and vertical centering, red arrow: maximum*

The curve depicts the symmetry of the cell. The maximum describes the drilled hole with the sample, whereas the shoulders describe the sample carrier. The cell is then shifted in a way, that the maximum of the curve (figure 5.4, red arrow) is in the center of the recording. To center the cell in beam direction, several measurements at different angle positions are performed. By determining the positions of maximum intensity, the correction for the centering in beam direction is calculated using trigonometry. After centering, the diode is moved back out of the arrangement and the sample is ready for the measurements.

For recording the program QXRD Readout Software V0.9.9 is used, which was developed for the

recording with Perkin Elmer area detectors by Dr. Guy Jennings at the Argonne National Laboratory. It offers a graphical user interface for the control of the detector. The recordings are saved in the tiff format. They show rings as in a Debye-Scherer camera, which depict intensity maxima of the diffracted radiation. Such a recording is shown in figure 5.5. The coarse granulation can be explained as reflexes of single crystals by the strong focusing of the beam.

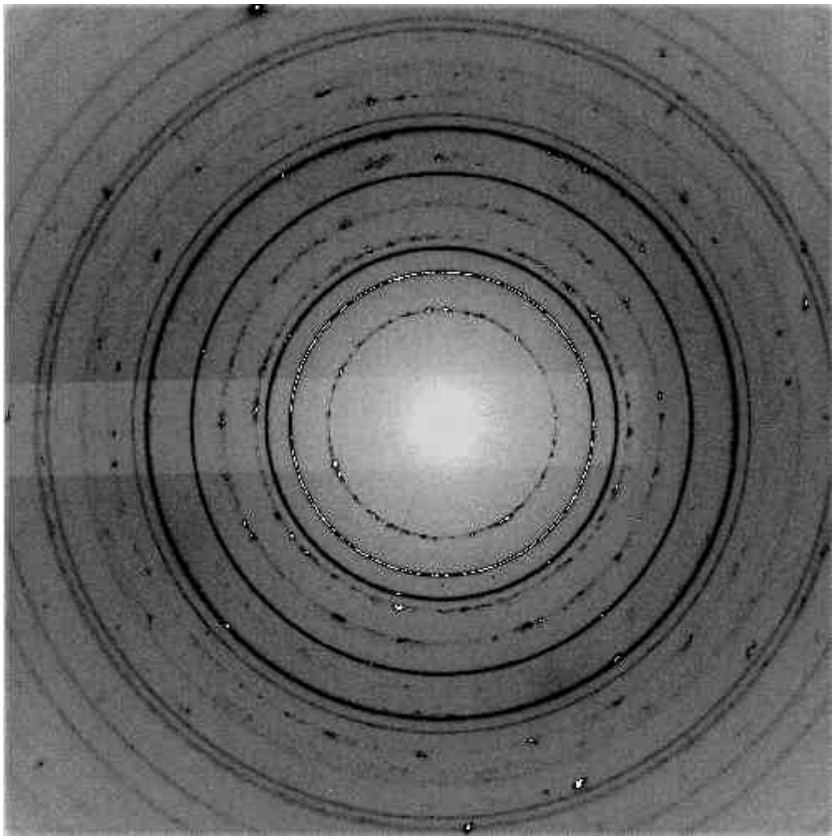

***Figure 5.5**: recording 001 of run07 with QXRD Readout Software V0.9.9 in the tiff format with typical ring pattern, the coarse granulation can be explained as reflexes of single crystals by the strong focusing of the beam*

For the measurement, a suitable site of the sample is selected. For this purpose, the sample is moved horizontally and vertically. Simultaneously individual recordings are taken and analyzed with the program GSE_shell V1.04. Silicon should be seen with a higher intensity than gold. Sometimes it can't be prevented to measure the diamonds of the diamond anvil cell, which is no problem for the evaluation. A dark image of the selected position is recorded with QXRD Readout

Software V0.9.9.

Before starting the measurement, the pressure profile on the He-membrane for the experiment must be programmed. A generic pressure profile is shown in diagram 5.1. To ensure contact between the He-membrane and the diamond anvil cell, the experiment starts with 3 bar. This arises no pressure on the sample itself.

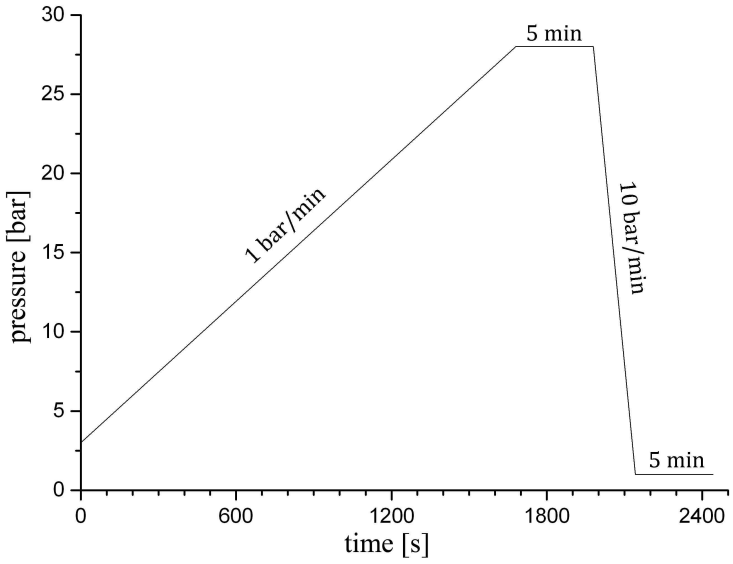

***Diagram 5.1**: programmed generic pressure profile on the He-membrane*

After programming the pressure profile, the required number of images must be calculated using the following formula:

$$N_{images} = t_{experiment}/t_0$$

With N_{images} being the needed amount of pictures, $t_{experiment}$ being the time of the experiment given by the pressure profile and t_0 being the exposure time of the images. The obtained number of images is then entered in the program QXRD Readout Software V0.9.9. Thereupon the measurement can be started with the recording of the images and the application of the pressure profile simultaneously.

5.5 Evaluation

For the analysis of the recordings several programs and graphical user interfaces are used. Figure 5.6 shows a flow chart of the sequence of analysis. A distinction is made with an overview and an analysis path.

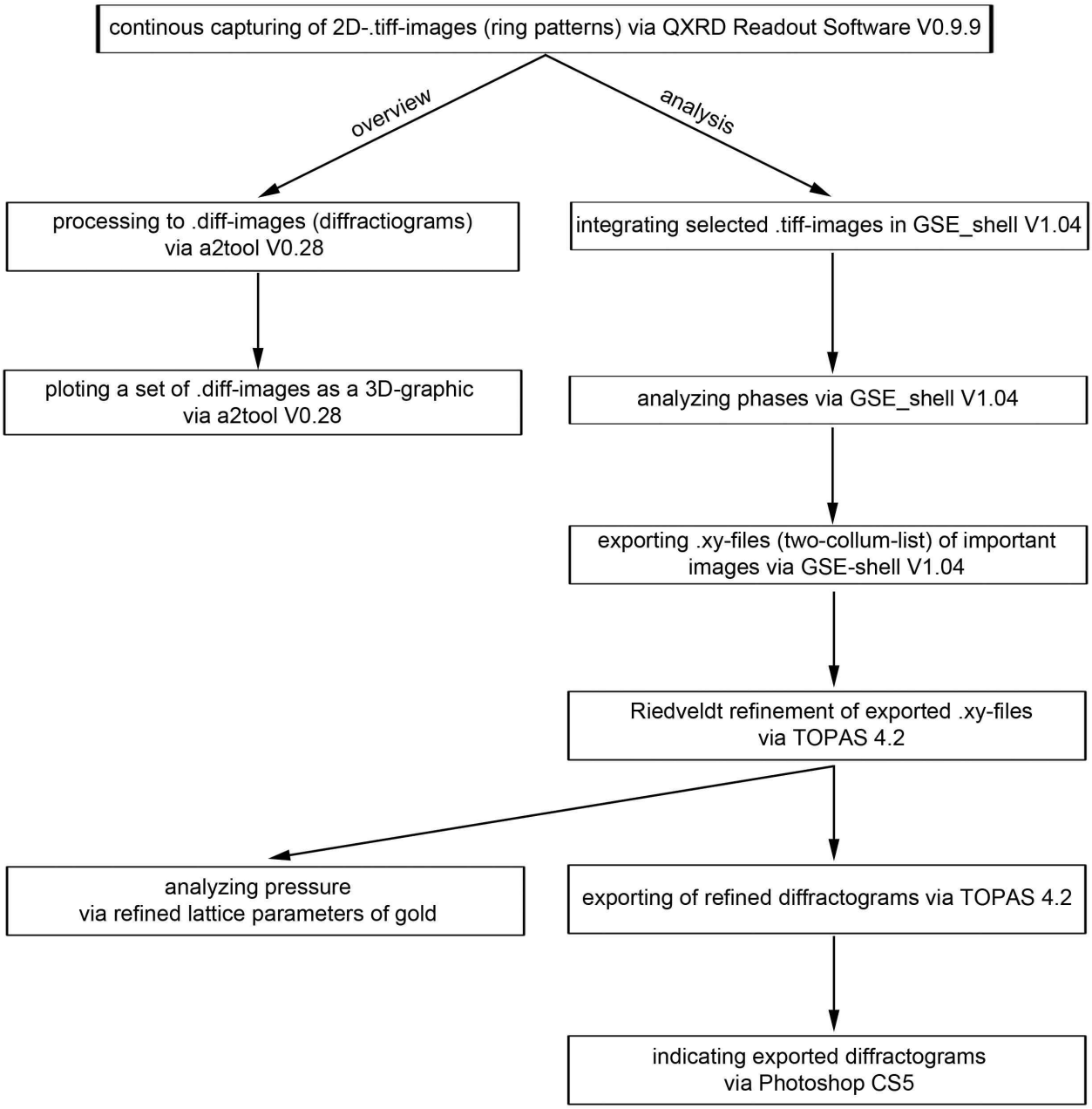

***Figure 5.6**: flow chart of the evaluation with overview and analysis path*

Before starting the evaluation, the programs must be calibrated to the used radiation. For a quick and easy presentation and overview of the data, the program a2tool V0.28 is used. The program was developed by Dr. Andre Rothkirch at DESY and allows a presentation of the experiments as 3D graphics. For this purpose, the calibration needs to be entered in the program. Then the data can be processed from the tiff format to the diff format. The circular diffraction reflexes are transformed into a diffraction pattern by integration. Due to the short wavelength of λ = 0.28988 Å, the resulting diffraction patterns cover only a small 2Θ-range, which can be derived from equation 3.2. The continuous images are then put in succession and can be viewed and rotated as a 3D graphics.

A more precise examination of the data can be performed with the program GSE_shell V1.04. The individual images are shown as diffraction patterns by integration. By overlaying with hkl values of certain phases, as shown in figure 5.3, the contained modifications can be analyzed. By simulating the shift of the hkl values caused by pressure dependence, an overview of the actual pressure profile by gold can be made.

For the analysis of the data using the Rietveld refinement, the program TOPAS 4.2 by Bruker is used. To import the data in TOPAS, they need to be exported in the program GSE_shell V1.04 in the chi format. In this format, the data are saved in two columns, 2Θ and intensity. The file extension .chi has to be replaced by .xy for the import in TOPAS. Table 5.2 shows the used settings for the Rietveld refinement in TOPAS.

Table 5.2*: used settings for the rietveld refinement in the program TOPAS 4.2*

Range	Parameter	Value
Emission Profile	Area	1
	WL(Å)	0.28988
	Lortz. HW	1

Background	Point detector	-
	Finger_et_al	S(mm) 2 refine
		H(mm) 3 refine
Corrections	Zero error	0 refine
	LP factor	90
Miscellaneous	Fixed WL Neutron	-
CIF	Peak Type	PV_TCHZ
	Gitterparameter	refine
	Scale	variabel refine

Since in TOPAS and other programs no satisfying correction for the synchrotron underground radiation was available, its effect for the analysis was minimized by cutting off the flanks of the diffraction patterns in TOPAS as seen in figure 5.7.

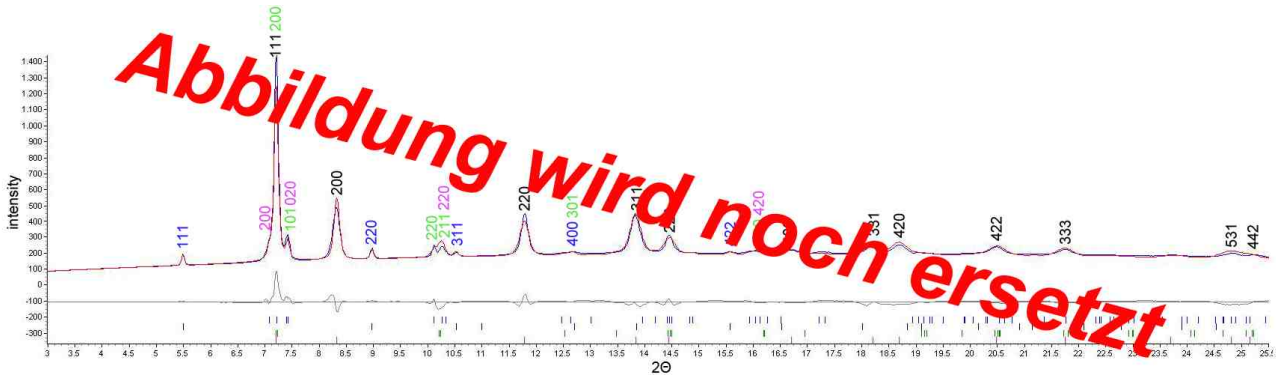

***Figure 5.7**: cutting of the flanks of the diffraction patterns in TOPAS to minimize the effect of the underground radiation*

For the analysis of the different phases, CIF files are imported in TOPAS. These were downloaded from the Crystallography Open Database (COD). For the use in TOPAS, they got checked and edited with the program enCIFer Version 1.4 of the Cambridge Crystallographic Data Centre (CCDC). Table 5.3 shows the used CIF files with their respective references. Since no CIF file was

available for Si II, it was created using enCIFer Version 1.4.

***Table 5.3**: used CIF files with their respective references for all phases*

Phase	COD number	Reference
Si I	9013102	(Dutta, 1962)
Si II	-	(Hu & Spain, 1984)
Si XI	9011656	(McMahon & Nelmes, 1993)
Si V	9012918	(Olijnyk *et al.*, 1984)
Si VI	9011645	(Hanfland *et al.*, 1999)
Au	9008463	(Wyckoff, 1982)

Since TOPAS is not able to adjust the lattice parameters at high pressures autonomously, they need to be manually pre-adjusted for the Rietveld refinement. Values are set for the individual lattice parameters, which are closer to the expected parameters than the ones of the phase at normal pressure. As a measure of accuracy of the refinement the GOF (goodness of fit) is given by TOPAS. The smaller the value, the better the fit. The refined diffraction patterns are exported and indexed with Photoshop CS5. For this purpose, the indices of the individual peaks are extracted from the program GSE_shell V1.04. For obscurities and the indexing of the phase Si VI, the indices are extracted from the program PowderCell 2.4. It was programmed by Dipl.-Ing. W. Kraus and Dr. G. Nolze at the Federal Institute of Materials Research and Testing in Berlin.

Due to the strong focusing of the radiation and the poor homogenization of the sample, only a low weighting is placed on the quantitative amounts of the values obtained by the Rietveld refinement. The analysis is focused on the crystal structure refinement and the resulting pressure fields of the phases calculated with gold.

6 RESULTS

6.1 Overview

The following table 6.1 gives an overview of the experiments conducted, called runs, with the respective samples and programmed pressures on the He-membrane.

***Table 6.1**: overview of the conducted experiments, programmed pressures on the He-membrane*

Run	Sample	Pressure build-up [bar/min]	Pressure relief [bar/min]	Diamond anvil cell number
01	Si-wafer	1	4	5
02	Si-nanopowder	-	-	4
03	Si-standard	1	1	6
04	Si-nanopowder	1	-	4
05	Si-standard	1	1	5
06	Si-wafer	1	1	6
07	Si-standard	1	10	5
08	Si-wafer	1	10	6
09	Si-standard	10	10	5
10	Si-wafer	10	10	6
11	Si-standard	20	20	5
12	Si-standard	1	1	4
13	Si-wafer	20	20	6

Since the extent of this thesis is limited, not all conducted experiments can be evaluated. The analysis is restricted to run07 and run11, which are highlighted in gray in table 6.1. With an pressure build-up of 1 bar/min, run07 gives a good overview of the phase transitions. Run11 can be considered as a comparison with the same sample and a fast pressure build-up of 20 bar/min.

6.2 Low pressure gradient - run07

For run07, the diamond anvil cell number 5 was loaded with the sample Si-standard. As shown in

diagram 6.1, a pressure gradient on the He-membrane of 1 bar/min for pressure build-up and 10 bar/min for pressure relief was defined. The maximum pressure of 28 bar was maintained over a period of 5 min. After pressure relief, the sample was measured for another 5 min.

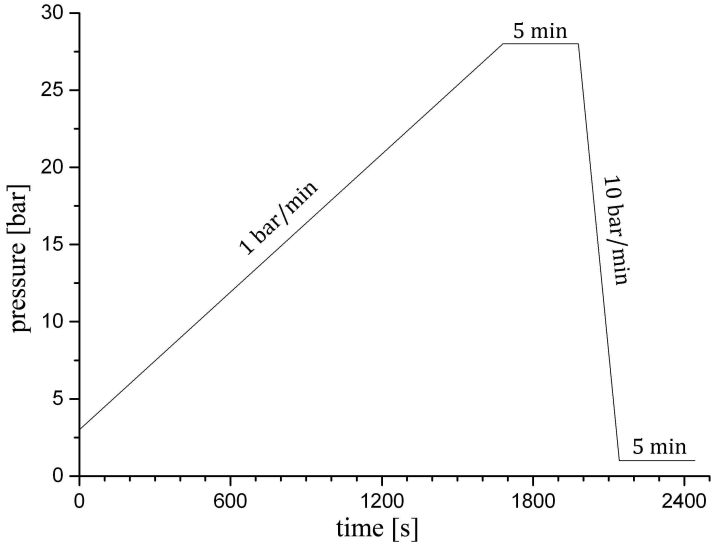

***Diagram 6.1**: programmed pressure profile on the He-membrane of run07*

The 3D graphics, figure 6.1, gives an overview of the experiment. In section A the pressure build-up of the experiment can be seen, based on the obvious shift of the peaks to higher 2Θ-values with time. In the following section B no further shift of the peaks occurs, which indicates a constant pressure. In this section of the experiment the maximum pressure was maintained. In the first part of section C the pressure relief takes place, which again can be seen by the shift of the peaks to lower 2Θ-values with time. The second part of section C indicates constant pressure. No complete pressure relief is possible due to the diamond anvil cell getting stuck. Thus the peaks can not shift back to their original 2Θ-values.

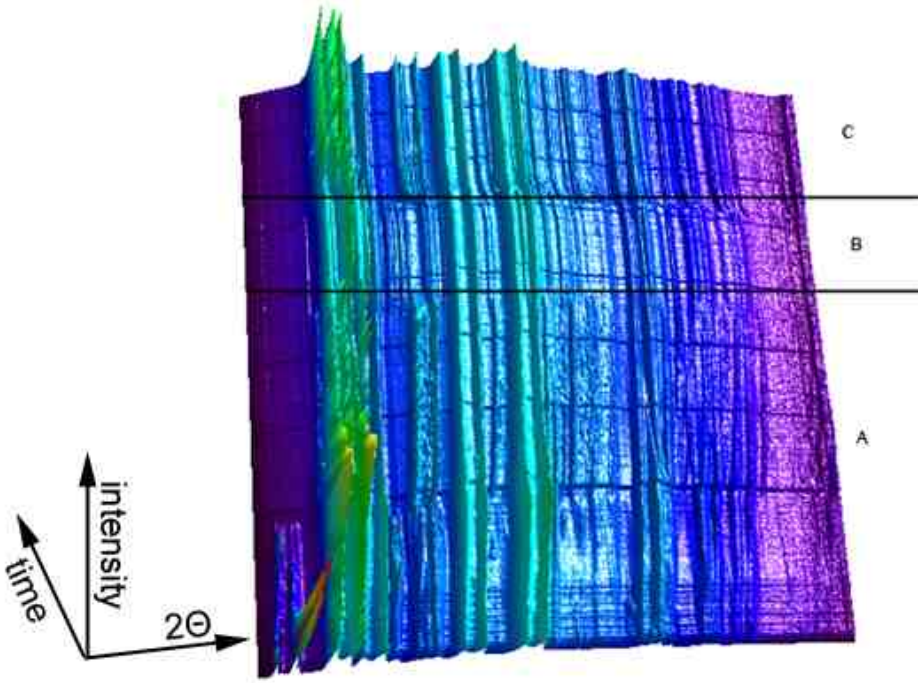

***Figure 6.1**: 3D graphics of run07 from 5° to 27° 2Θ, A: pressure build-up, B: maximum pressure, C: pressure relief*

Diagram 6.2 shows the pressure on the sample of the experiment by gold. The mean pressure gradient at pressure build-up is 1.57 GPa/min, at pressure relief 2.7 GPa/min. A maximum pressure of 40.5 GPa is reached. At pressure relief the diamond anvil cell gets stuck at 27 GPa.

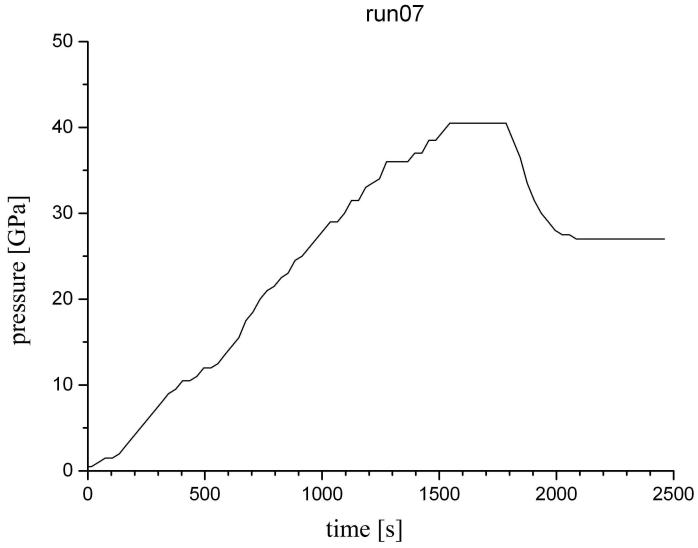

***Diagram 6.2**: actual pressure profile on the sample of run07 by gold*

For the qualitative and quantitative analysis of the experiment, individual diffraction patterns at distinctive locations are evaluated with the Rietveld method in the program TOPAS 4.2. In figure 6.2 a 3D graphics from 5° to 11° 2Θ is shown, in which arrows mark the positions of the individual diffraction patterns. For the refinement only a range of 3° to 25.5° 2Θ was used, because of the significant improvement of the fit. Thus, the effect of the strong underground radiation is minimized. Amongst the data of the individual refinements, the goodness of fit (GOF) is given as a measure of accuracy.

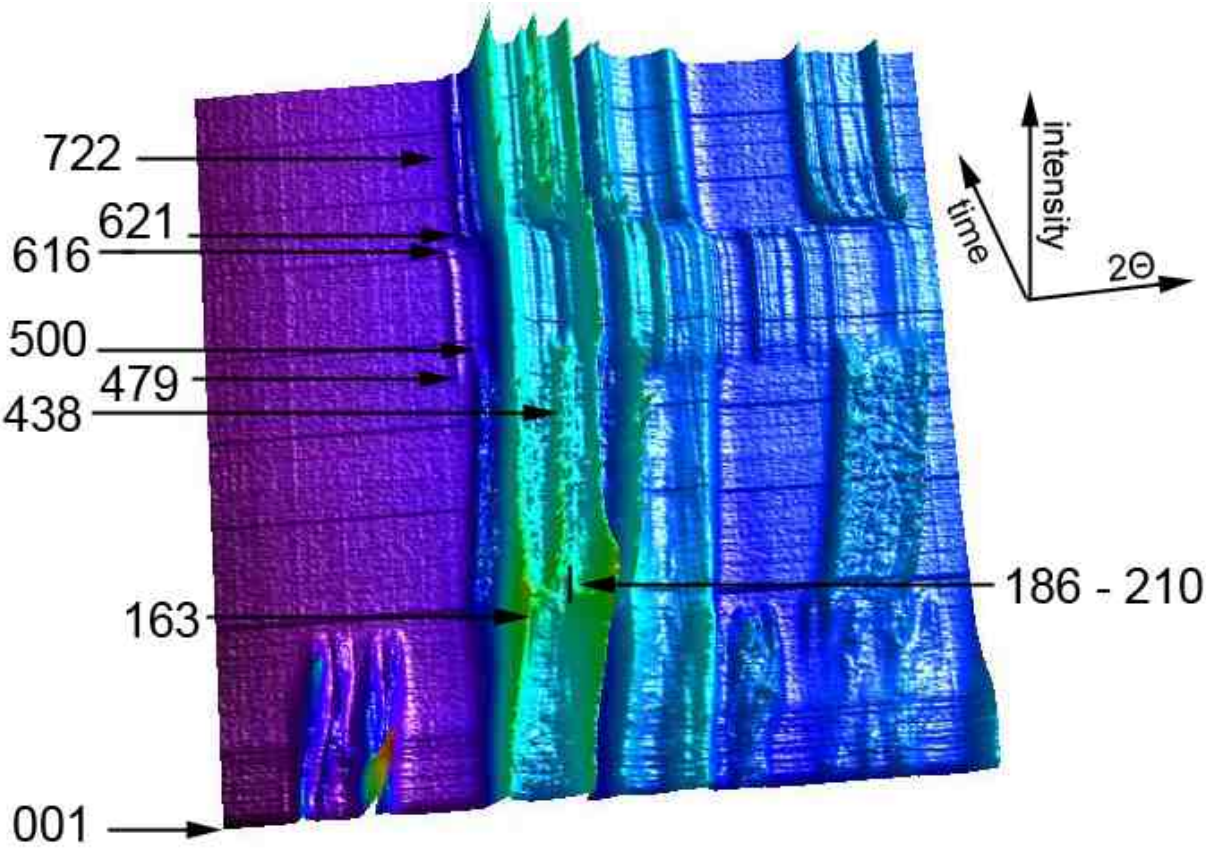

***Figure 6.2**: 3D graphics of run07 from 5° to 11° 2Θ, the arrows mark the positions of the refined diffraction patterns*

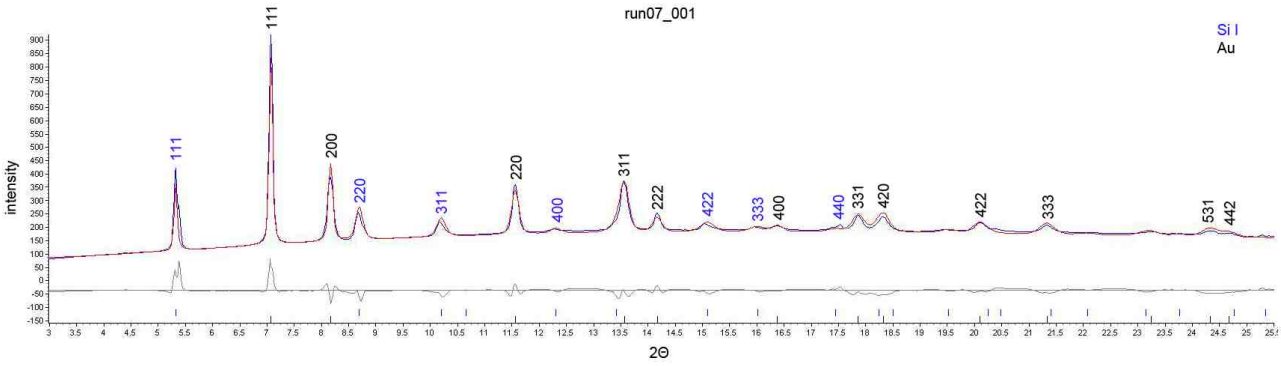

***Figure 6.3**: diffraction pattern of run07 recording 001, at a pressure of 1.12 GPa by gold Si I is stable*

Figure 6.3 shows the refined diffraction pattern of run07 recording 001. The following values were determined using the Rietveld method:

***Table 6.2**: values of the Rietveld refinement of run07 recording 001 (GOF = 0.62)*

Phase	Lattice parameters [Å]	Quantitative portion [%]
Au	a = 4.0696594 ± 0.0007400	82
Si I	a = 5.4070292 ± 0.0013948	18

The measurement represents the initial state of the sample and is a reference for the experiment. The phase Si I is stable at a pressure of 1.12 GPa by gold.

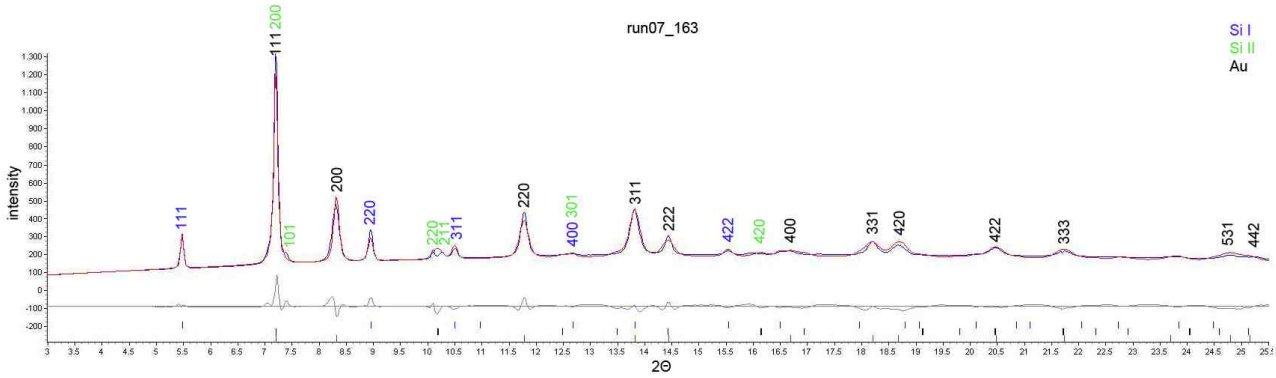

***Figure 6.4**: diffraction pattern of run07 recording 163, at a pressure of 12.35 GPa by gold Si I and Si II are stable, first occurrence of Si II*

Figure 6.4 shows the refined diffraction pattern of run07 recording 163. The following values were determined using the Rietveld method:

***Table 6.3**: values of the Rietveld refinement of run07 recording 163 (GOF = 0.64)*

Phase	Lattice parameters [Å]	Quantitative portion [%]
Au	a = 3.9945666 ± 0.0006906	85
Si I	a = 5.2515019 ± 0.0012408	8
Si II	a = 4.6154555 ± 0.0042526	7
	c = 2.6659171 ± 0.0051101	

The measurement marks the first occurrence of Si II. At a pressure of 12.35 GPa by gold Si I and Si II are stable.

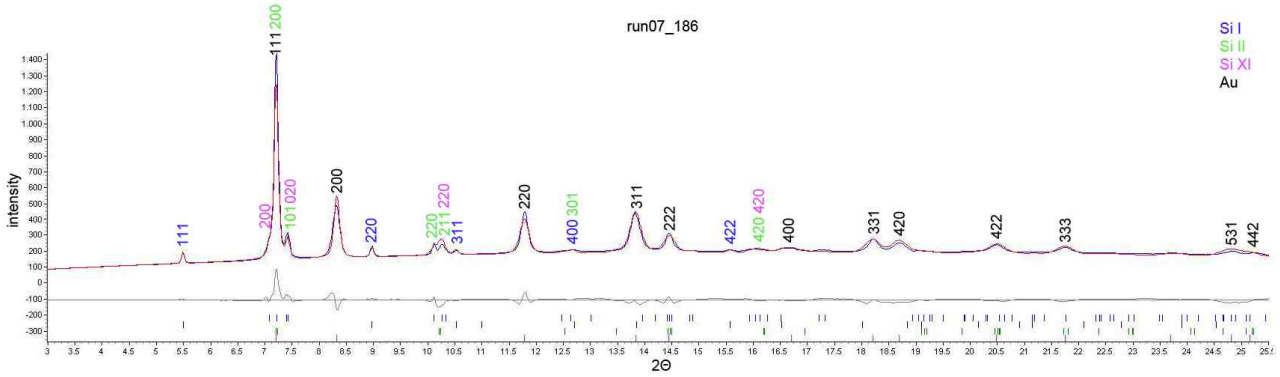

***Figure 6.5**: diffraction pattern of run07 recording 186, at a pressure of 12.70 GPa by gold Si I, Si II and Si XI are stable, first occurrence of Si XI*

Figure 6.5 shows the refined diffraction pattern of run07 recording 186. The following values were determined using the Rietveld method:

***Table 6.4**: values of the Rietveld refinement of run07 recording 186 (GOF = 0.64)*

Phase	Lattice parameters [Å]	Quantitative portion [%]
Au	a = 3.9926370 ± 0.0007198	85
Si I	a = 5.2391507 ± 0.0020559	2
Si II	a = 4.5966933 ± 0.0060116	5
	c = 2.6690195 ± 0.0067943	
Si XI	a =4.6932018 ± 0.0026909	8
	b = 4.6060406 ± 0.0054898	
	c = 2.5591480 ± 0.0014827	

The measurement marks the first occurrence of Si XI. At a pressure of 12.70 GPa by gold Si I, Si II and Si XI are stable.

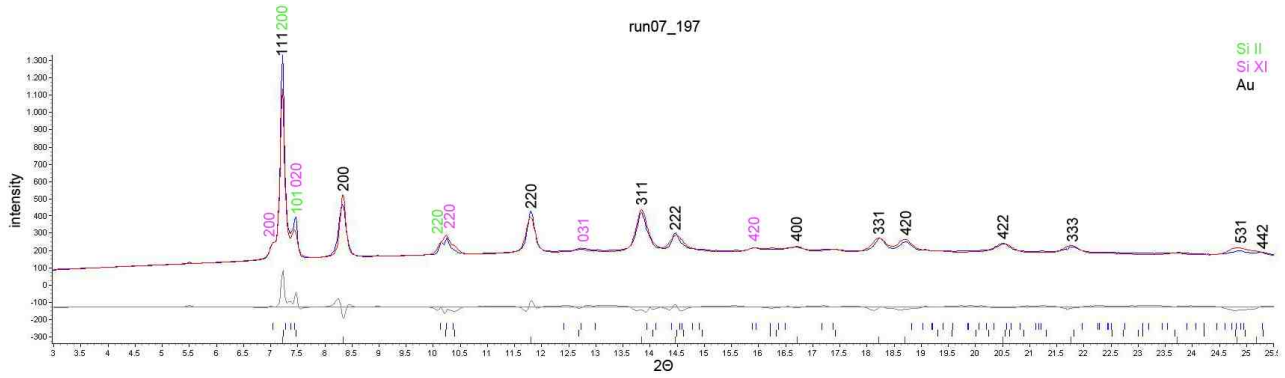

***Figure 6.6**: diffraction pattern of run07 recording 197, at a pressure of 13.12 GPa by gold Si II and Si XI are stable, first recording without Si I*

Figure 6.6 shows the refined diffraction pattern of run07 recording 197. The following values were determined using the Rietveld method:

***Table 6.5**: values of the Rietveld refinement of run07 recording 197 (GOF = 0.66)*

Phase	Lattice parameters [Å]	Quantitative portion [%]
Au	a = 3.9901885 ± 0.0008346	83
Si II	a = 4.5962181 ± 0.0078772	5
	c = 2.5455149 ± 0.0045636	
Si XI	a = 4.7241673 ± 0.0033629	12
	b = 4.5653391 ± 0.0049231	
	c = 2.5635127 ± 0.0023317	

This measurement marks the upper boundary of the pressure region of Si I. At a pressure of 13.12 GPa by gold Si II and Si XI are stable.

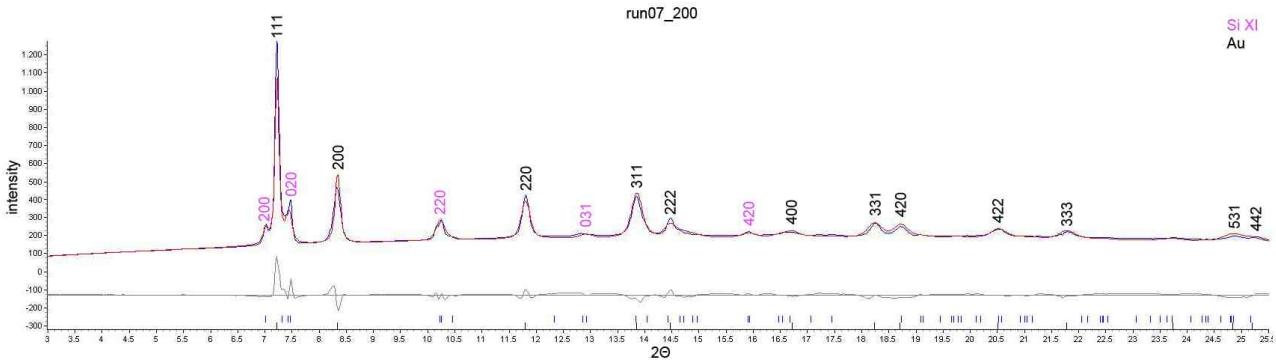

***Figure 6.7**: diffraction pattern of run07 recording 200, at a pressure of 13.55 GPa by gold Si XI is stable, upper boundary of the pressure region of Si II*

Figure 6.7 shows the refined diffraction pattern of run07 recording 200. The following values were determined using the Rietveld method:

***Table 6.6**: values of the Rietveld refinement of run07 recording 200 (GOF = 0.67)*

Phase	Lattice parameters [Å]	Quantitative portion [%]
Au	a = 3.9878446 ± 0.0011505	86
Si XI	a = 4.7411386 ± 0.0026972	14
	b = 4.4512149 ± 0.0057772	
	c = 2.5898069 ± 0.0033639	

The measurement marks the upper boundary of the pressure region of Si II. At a pressure of 13.55 GPa by gold Si XI is stable.

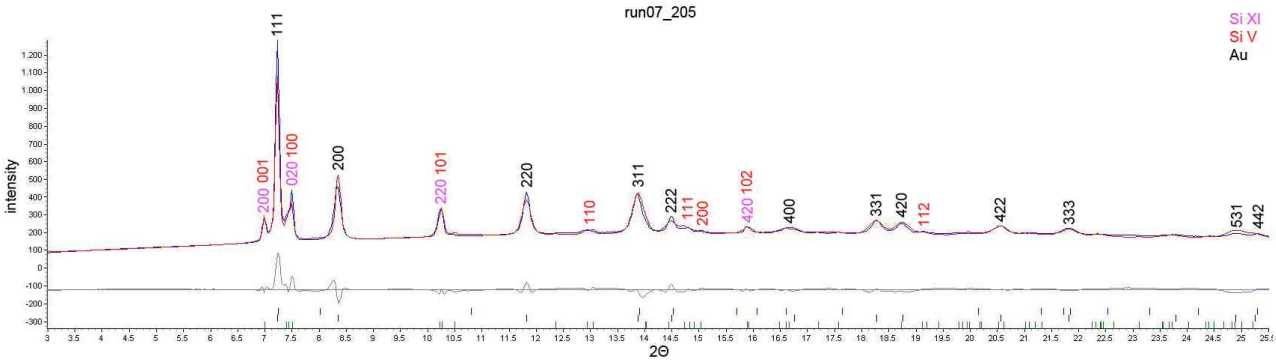

***Figure 6.8**: diffraction pattern of run07 recording 205, at a pressure of 15.22 GPa by gold Si XI and Si V are stable, first occurrence of Si V*

Figure 6.8 shows the refined diffraction pattern of run07 recording 205. The following values were determined using the Rietveld method:

***Table 6.7**: values of the Rietveld refinement of run07 recording 205 (GOF = 0.69)*

Phase	Lattice parameters [Å]	Quantitative portion [%]
Au	a = 3.9786475 ± 0.0007740	83
Si XI	a = 4.7514376 ± 0.0014001	14
	b = 4.4678346 ± 0.0018723	
	c = 2.5503502 ± 0.0009257	
Si V	a = 2.3953613 ± 0.01463779	3
	c = 2.2940082 ± 0.0241519	

The measurement marks the first occurrence of Si V. At a pressure of 15.22 GPa by gold Si XI and Si V are stable.

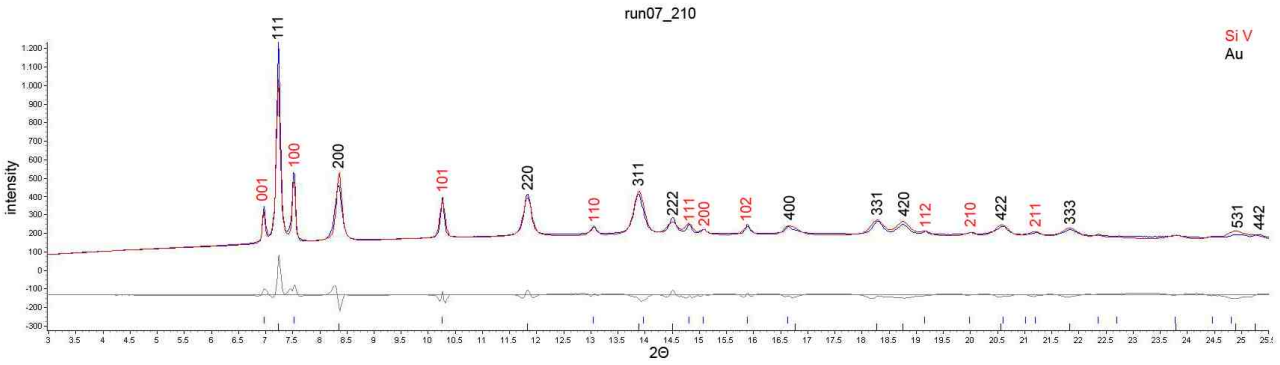

***Figure 6.9**: diffraction pattern of run07 recording 210, at a pressure of 15.37 GPa by gold Si V is stable, upper boundary of the pressure region of Si XI*

Figure 6.9 shows the refined diffraction pattern of run07 recording 210. The following values were determined using the Rietveld method:

***Table 6.8**: values of the Rietveld refinement of run07 recording 210 (GOF = 0.66)*

Phase	Lattice parameters [Å]	Quantitative portion [%]
Au	a = 3.9778399 ± 0.0006603	86
Si V	a = 2.5515325 ± 0.0005182	14
	c = 2.3843458 ± 0.0005604	

The measurement marks the upper boundary of the pressure region of Si XI. At a pressure of 15.37 GPa by gold Si V is stable.

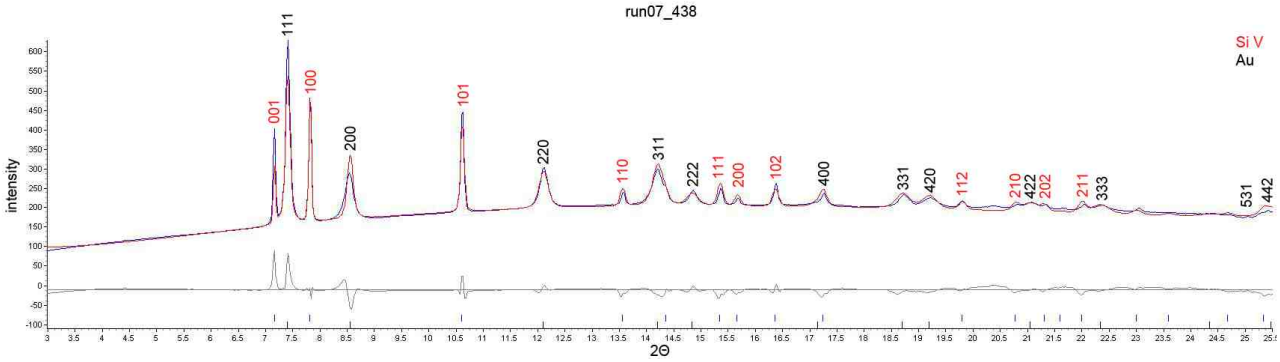

***Figure 6.10**: diffraction pattern of run07 recording 438, at a pressure of 35.20 GPa by gold Si V is stable*

Figure 6.10 shows the refined diffraction pattern of run07 recording 438. The following values were determined using the Rietveld method:

***Table 6.9**: values of the Rietveld refinement of run07 recording 438 (GOF = 0.48)*

Phase	Lattice parameters [Å]	Quantitative portion [%]
Au	a = 3.8890245 ± 0.0007194	80
Si V	a = 2.4566346 ± 0.0004453	20
	c = 2.3206249 ± 0.0004510	

At a pressure of 35.20 GPa the phase Si V is stable.

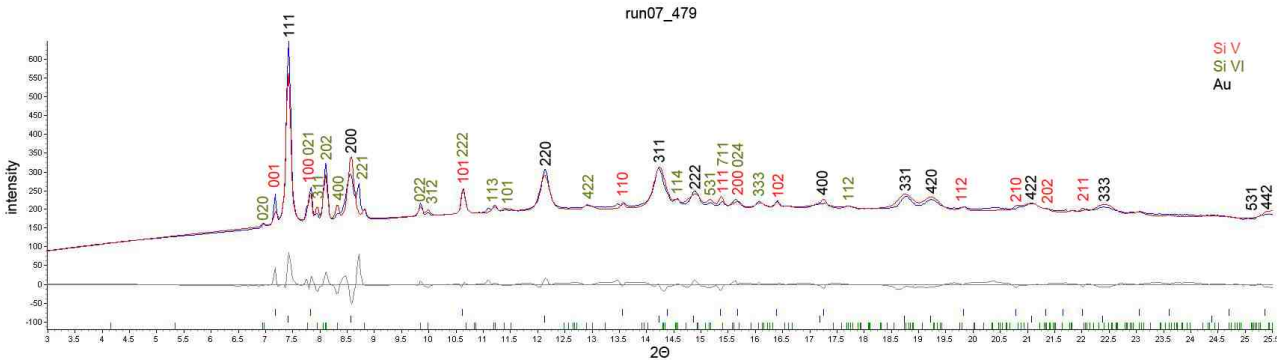

***Figure 6.11**: diffraction pattern of run07 recording 479, at a pressure of 37.13 GPa by gold Si V and Si VI are stable, first occurrence of Si VI*

Figure 6.11 shows the refined diffraction pattern of run07 recording 479. The following values were determined using the Rietveld method:

***Table 6.10**: values of the Rietveld refinement of run07 recording 479 (GOF = 0.48)*

Phase	Lattice parameters [Å]	Quantitative portion [%]
Au	a = 3.8818002 ± 0.0012518	81
Si V	a = 2.4549476 ± 0.0008485	6
	b = 2.3150761 ± 0.0010845	
Si VI	a = 7.9977593 ± 0.0039659	13
	b = 4.7869592 ± 0.0036265	
	c = 4.7703670 ± 0.0036220	

The measurement marks the first occurrence of Si VI. At a pressure of 37.13 GPa by gold Si V and Si VI are stable.

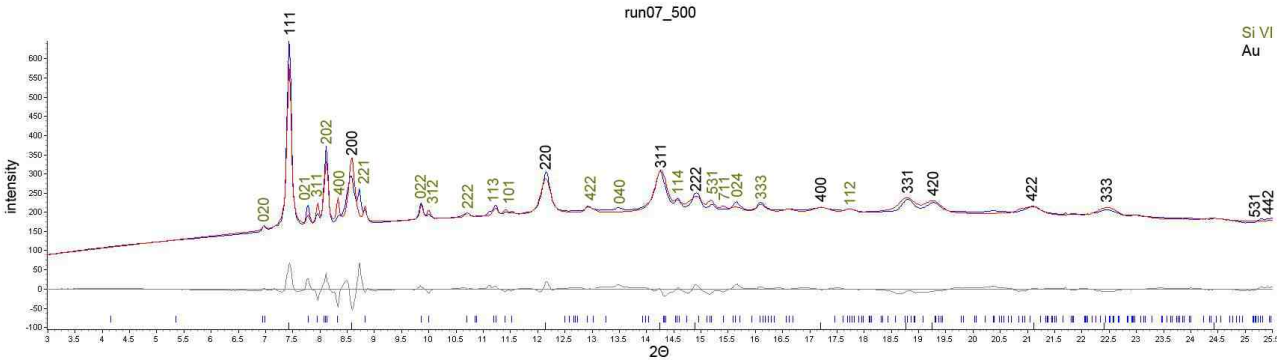

***Figure 6.12**: diffraction pattern of run07 recording 500, at a pressure of 38.67 GPa by gold Si VI is stable, upper boundary of the pressure region of Si V*

Figure 6.12 shows the refined diffraction pattern of run07 recording 500. The following values were determined using the Rietveld method:

***Table 6.11**: values of the Rietveld refinement of run07 recording 500 (GOF = 0.47)*

Phase	Lattice parameters [Å]	Quantitative portion [%]
Au	a = 3.8762159 ± 0.0008905	82
Si VI	a = 7.9898439 ± 0.0026384	18
	b = 4.7844262 ± 0.0018971	
	c = 4.7619738 ± 0.0021529	

The measurement marks the upper boundary of the pressure region of Si V. At a pressure of 38.67 GPa by gold Si VI is stable.

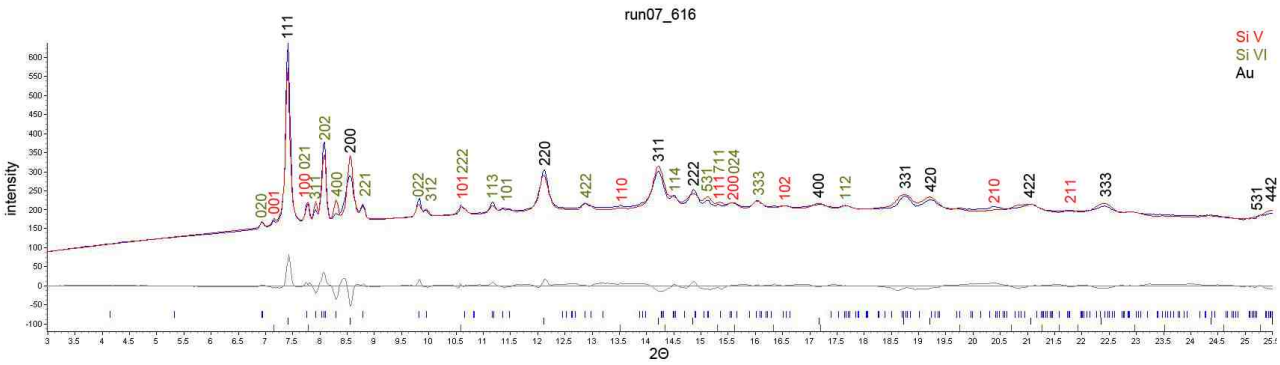

***Figure 6.13**: diffraction pattern of run07 recording 616, at a pressure of 36.29 GPa by gold Si V and Si VI are stable, first occurrence of Si V on pressure relief*

Figure 6.13 shows the refined diffraction pattern of run07 recording 616. The following values were determined using the Rietveld method:

***Table 6.12**: values of the Rietveld refinement of run07 recording 616 (GOF = 0.41)*

Phase	Lattice parameters [Å]	Quantitative portion [%]
Au	a = 3.8848830 ± 0.0008518	79
Si V	a = 2.4639775 ± 0.0011602	2
	c = 2.3228678 ± 0.0026491	
Si VI	a = 8.0128089 ± 0.0027966	19
	b = 4.7989741 ± 0.0027272	
	c = 4.7841285 ± 0.0028203	

The measurement marks the first occurrence of Si V on pressure relief. At a pressure of 36.29 GPa by gold Si V and Si VI are stable.

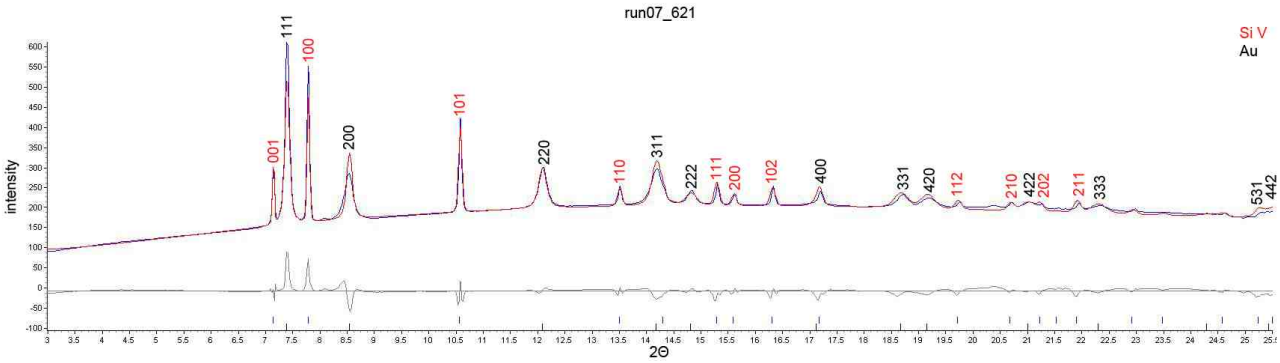

***Figure 6.14**: diffraction pattern of run07 recording 621, at a pressure of 33.34 GPa by gold Si V is stable, lower boundary of pressure region of Si VI on pressure relief*

Figure 6.14 shows the refined diffraction pattern of run07 recording 621. The following values were determined using the Rietveld method:

***Table 6.13**: values of the Rietveld refinement of run07 recording 621 (GOF = 0.46)*

Phase	Lattice parameters [Å]	Quantitative portion [%]
Au	a = 3.8961208 ± 0.0005622	82
Si V	a = 2.4672433 ± 0.0002974	18
	c = 2.3282388 ± 0.0003501	

The measurement marks the lower boundary of the pressure region of Si VI on pressure relief. At a pressure of 33.34 GPa Si V is stable.

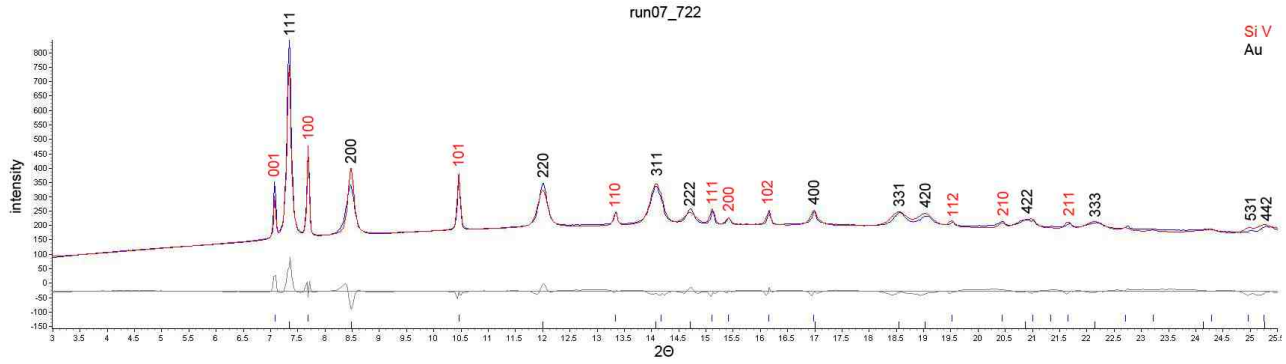

***Figure 6.15**: diffraction pattern of run07 recording 722, at a pressure of 27.12 GPa by gold Si V is stable*

Figure 6.15 shows the refined diffraction pattern of run07 recording 722. The following values were determined using the Rietveld method:

***Table 6.14**: values of the Rietveld refinement of run07 recording 722 (GOF = 0.48)*

Phase	Lattice parameters [Å]	Quantitative portion [%]
Au	a = 3.9214609 ± 0.0005477	88
Si V	a = 2.4956952 ± 0.0002929	12
	c = 2.3484881 ± 0.0003434	

The measurement is the last of the experiment. At a pressure of 27.12 GPa by gold the phase Si V

is stable.

The analysis of the data resulted in the following sequence of phases with increasing pressure:

$$Si\ I(< 13.0) \rightarrow Si\ II(12.0 - 13.5) \rightarrow Si\ XI(12.5 - 15.0) \rightarrow Si\ V(15.0 - 38.5) \rightarrow Si\ VI(37.0 - min.38.67)$$

The numbers in brackets indicate the respective rounded pressure range in GPa, in which the phases occur. Some multiphase fields with up to three simultaneously existing phases occur. In diagram 6.3, the percentages of the individual Si phases minus the gold content are plotted against the pressure, calculated by gold. Thus can be seen, that Si II is the only phase not occurring alone.

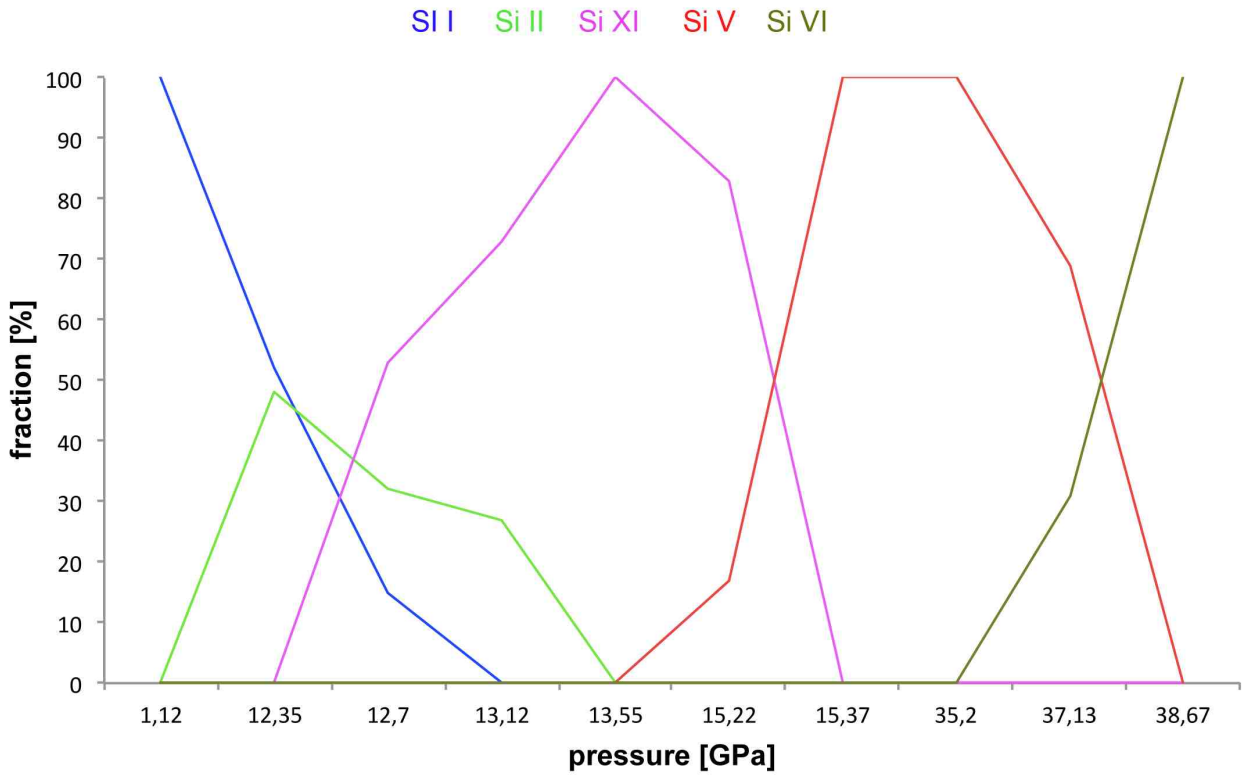

***Diagramm 6.3**: run07, percentages of the individual Si phases against the pressure by gold, Si II is the only phase not occurring alone*

At pressure relief the pressure regions of Si V and Si VI shift to lower pressures. Si VI is present down to 34.0 GPa, Si V occurs only from 36.5 GPa.

6.3 High pressure gradient - run11

For run11 the diamond anvil cell number 5 was loaded with the sample Si-standard. As shown in diagram 6.4, a pressure gradient on the He-membrane of 20 bar/min at pressure build-up and 20 bar/min at pressure relief was programmed. The maximum pressure of 28 bar was maintained for 1 min. After pressure relief, the sample was measured for another 3 min.

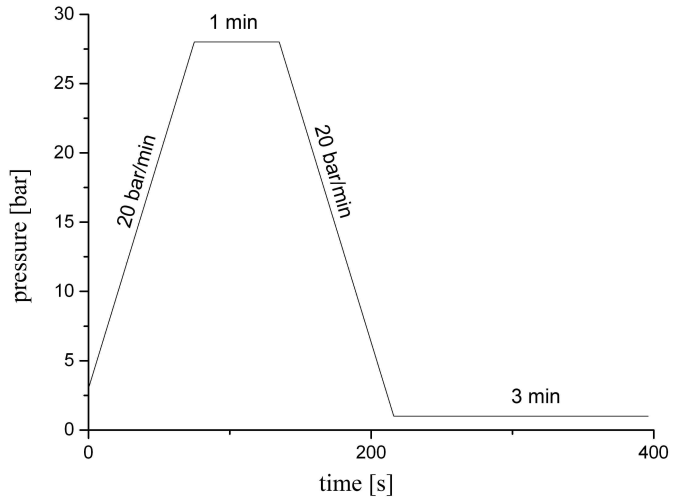

***Diagram 6.4**: programmed pressure profile on the He-membrane of run11*

Diagram 6.5 shows the actual pressure profile of the experiment by gold. At pressure build-up the mean pressure gradient is 44 GPa/min, at pressure relief 8.31 GPa/min. A maximum pressure of 34 GPa is reached. At pressure relief the diamond anvil cell gets stuck at 14.5 GPa.

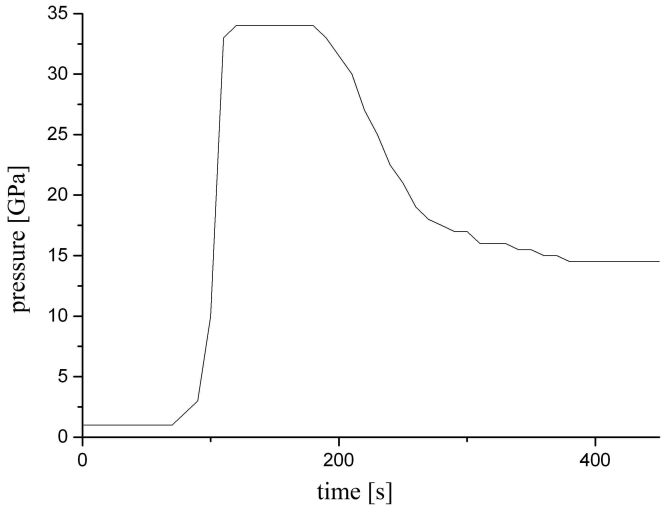

Diagram 6.5*: actual pressure profile by gold of run11*

As with run07 the change in pressure is seen by the shift of the peaks. For the qualitative and quantitative analysis of the experiment, individual diffraction patterns at distinctive locations are evaluated with the Rietveld method in the program TOPAS 4.2. Figure 6.16 shows a 3D graphics from 5° to 11° 2Θ, in which the arrows mark the positions of the individual diffraction patterns. For the refinement only a range of 3° to 24° 2Θ was used, because of the strong underground radiation and the diamond peak in the rear part of the diffraction pattern. Amongst the data of the individual refinements, the goodness of fit (GOF) is given as a measure of accuracy.

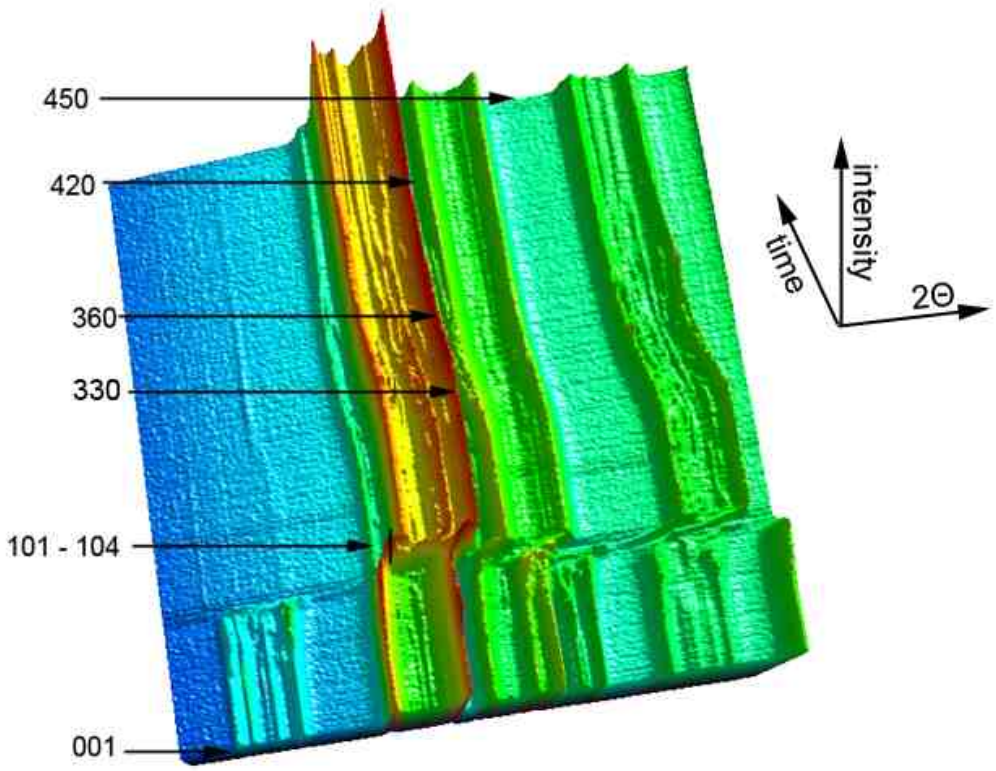

***Figure 6.16**: 3D graphics of run11 from 5° to 11° 2Θ, the arrows mark the positions of the refined diffraction patterns.*

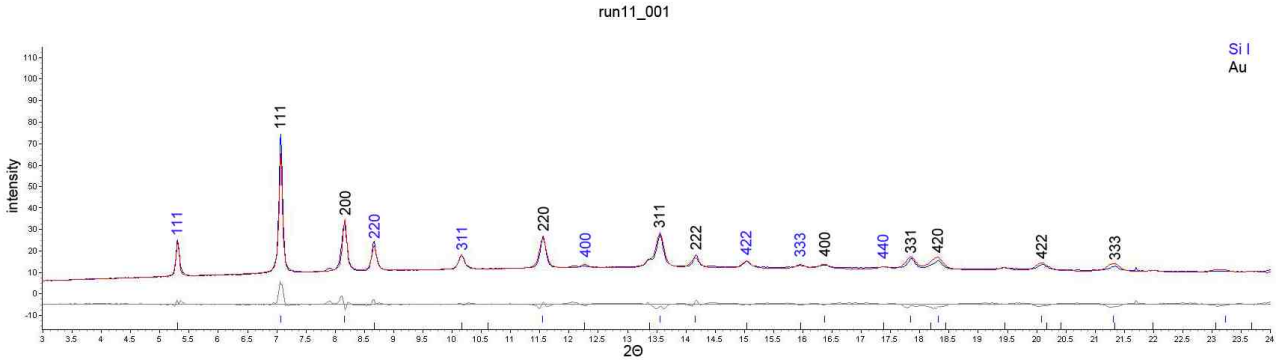

***Figure 6.17**: diffraction pattern of run11 recording 001, at a pressure of 0.66 GPa by gold Si I is stable*

Figure 6.17 shows the refined diffraction pattern of run11 recording 001. The following values were determined using the Rietveld method:

***Table 6.15**: values of the Rietveld refinement of run11 recording 001 (GOF = 0.16)*

Phase	Lattice parameters [Å]	Quantitative portion [%]
Au	a = 4.0733078 ± 0.0004878	86
Si I	a = 5.4261778 ± 0.0009243	14

The measurement represents the initial state of the sample and is a reference for the experiment. The phase Si I is stable at a pressure of 1.12 GPa by gold.

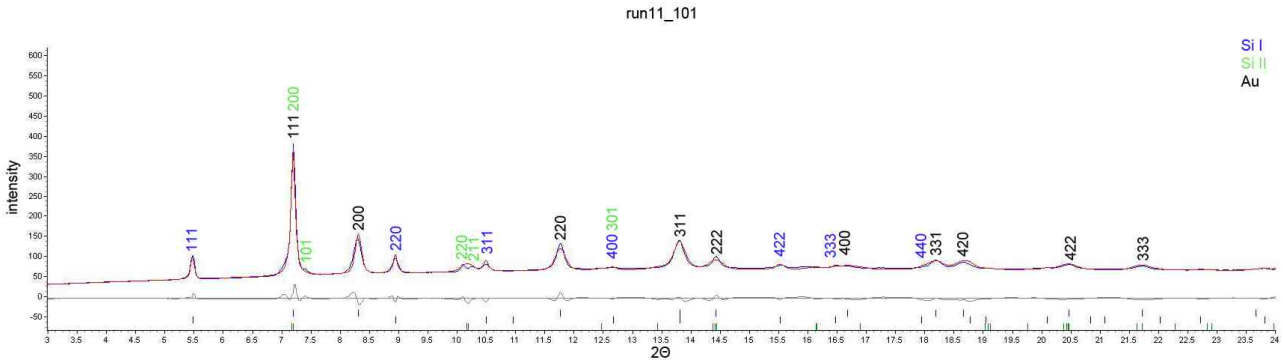

***Figure 6.18**: diffraction pattern of run11 recording 101, at a pressure of 11.72 GPa by gold Si I and Si II are stable, first occurrence of Si II*

Figure 6.18 shows the refined diffraction pattern of run11 recording 101. The following values were determined using the Rietveld method:

***Table 6.16**: values of the Rietveld refinement of run11 recording 101 (GOF = 0.32)*

Phase	Lattice parameters [Å]	Quantitative portion [%]
Au	a = 3.9982130 ± 0.0007537	81
Si I	a = 5.2555504 ± 0.0011668	9
Si II	a = 4.6152105 ± 0.0044160	10
	c = 2.6790992 ± 0.0053681	

The measurement marks the first occurrence of Si II. The phases Si I and Si II are stable at a pressure of 11.72 GPa by gold.

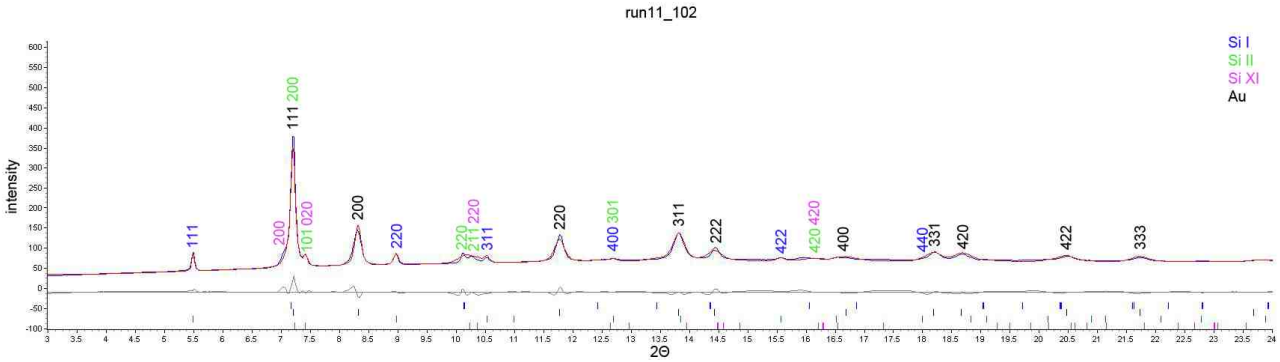

***Figure 6.19**: diffraction pattern of run11 recording 102, at a pressure of 11.95 GPa by gold Si I, Si II and Si XI are stable, first occurrence of Si XI*

Figure 6.19 shows the refined diffraction pattern of run11 recording 102. The following values were determined using the Rietveld method:

***Table 6.17**: values of the Rietveld refinement of run11 recording 102 (GOF = 0.31)*

Phase	Lattice parameters [Å]	Quantitative portion [%]
Au	a = 3.9969835 ± 0.0008312	81
Si I	a = 5.2418340 ± 0.0016012	5
Si II	a = 4.6404486 ± 0.0066837	10
	c = 2.6755383 ± 0.0066171	
Si XI	a = 4.5984526 ± 0.0126780	4
	b = 4.5969602 ± 0.0128949	
	c = 2.5661895 ± 0.0022132	

The measurement marks the first occurrence of Si XI. The phases Si I, Si II and Si XI are stable at a pressure of 11.95 GPa by gold.

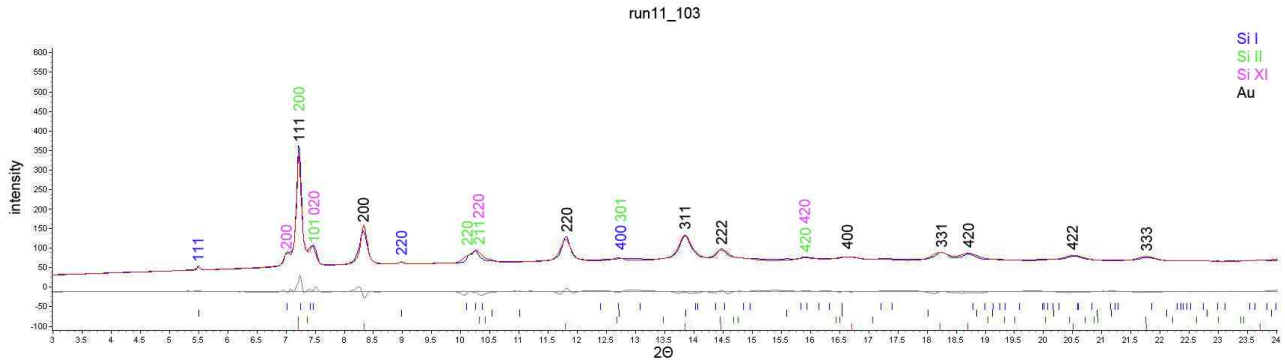

***Figure 6.20**: diffraction pattern of run11 recording 103, at a pressure of 13.33 GPa by gold Si I, Si II and Si XI are stable*

Figure 6.20 shows the refined diffraction pattern of run11 recording 103. The following values were determined using the Rietveld method:

***Table 6.18**: values of the Rietveld refinement of run11 recording 103 (GOF = 0.29)*

Phase	Lattice parameters [Å]	Quantitative portion [%]
Au	a = 3.9890878 ± 0.0008358	82
Si I	a = 5.2348556 ± 0.0035320	1
Si II	a = 4.5147947 ± 0.0083243	5
	c = 2.6793063 ± 0.0095080	
Si XI	a = 4.7375437 ± 0.0021657	12
	b = 4.5866252 ± 0.0043304	
	c = 2.5459715 ± 0.0014730	

The measurement marks the last occurrence of Si I, Si II and Si XI at a pressure of 13.33 GPa by gold.

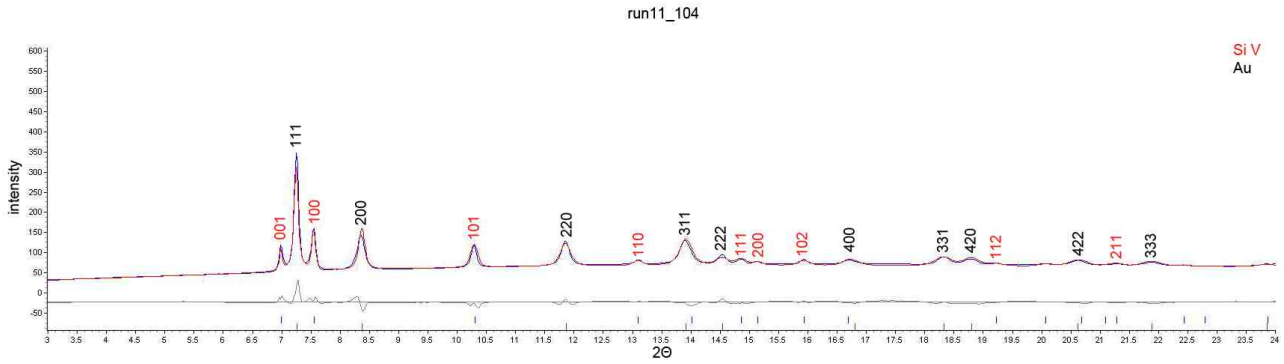

***Figure 6.21**: diffraction pattern of run11 recording 104, at a pressure of 17.29 GPa by gold Si V is stable, first occurrence of Si V*

Figure 6.21 shows the refined diffraction pattern of run11 recording 104. The following values were determined using the Rietveld method:

***Table 6.19**: values of the Rietveld refinement of run11 recording 104 (GOF = 0.33)*

Phase	Lattice parameters [Å]	Quantitative portion [%]
Au	a = 3.9677960 ± 0.0008025	84
Si V	a = 2.5411206 ± 0.0005920	16
	c = 2.3759933 ± 0.0006381	

The measurement marks the last occurrence of Si V at a pressure of 17.29 GPa by gold. Due to the high pressure gradient, the transitions between the different phases are not accurately recorded.

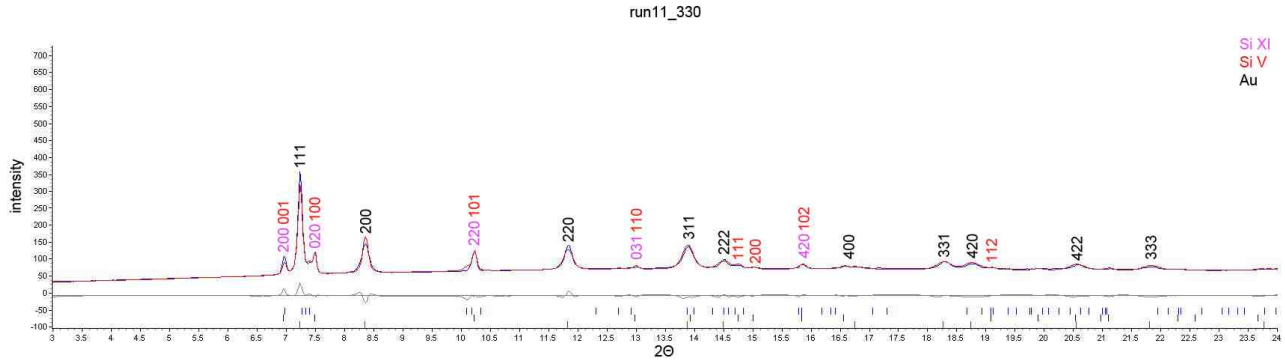

***Figure 6.22**: diffraction pattern of run11 recording 330, at a pressure of 14.78 GPa by gold Si XI and Si V are stable, first occurrence of Si XI at pressure relief*

Figure 6.22 shows the refined diffraction pattern of run11 recording 330. The following values were determined using the Rietveld method:

Table 6.20: values of the Rietveld refinement of run11 recording 330 (GOF = 0.30)

Phase	Lattice parameters [Å]	Quantitative portion [%]
Au	a = 3.9810981 ± 0.0007736	85
Si XI	a = 4.7610277 ± 0.0035303	8
	b = 4.5695501 ± 0.0054234	
	c = 2.5765395 ± 0.0027782	
Si V	a = 2.5636473 ± 0.0006859	7
	c = 2.3899480 ± 0.0011417	

The measurement marks the first occurrence of Si XI at a pressure of 14.78 GPa by gold at pressure relief. The phases Si XI and Si V are stable.

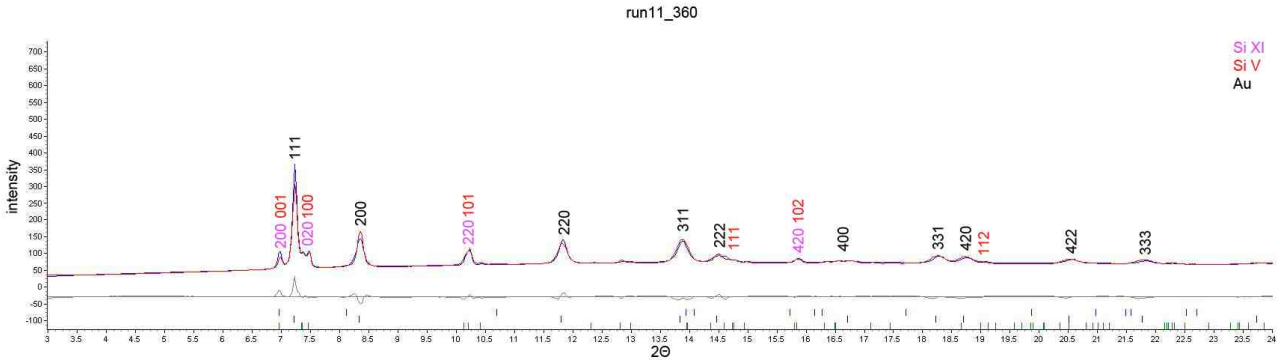

***Figure 6.23**: diffraction pattern of run11 recording 360, at a pressure of 13.42 GPa by gold Si XI and Si V are stable*

Figure 6.23 shows the refined diffraction pattern of run11 recording 360. The following values were determined using the Rietveld method:

***Table 6.21**: values of the Rietveld refinement of run11 recording 360 (GOF = 0.33)*

Phase	Lattice parameters [Å]	Quantitative portion [%]
Au	a = 3.9885771 ± 0.0009673	85
Si XI	a = 4.7706790 ± 0.0016756	14
	b = 4.5205855 ± 0.0017919	
	c = 2.5617261 ± 0.0008787	
Si V	a = 2.3655950 ± 0.0096423	1
	c = 2.3887565 ± 0.0183127	

At a pressure of 13.42 GPa by gold the phases Si XI and Si V are stable.

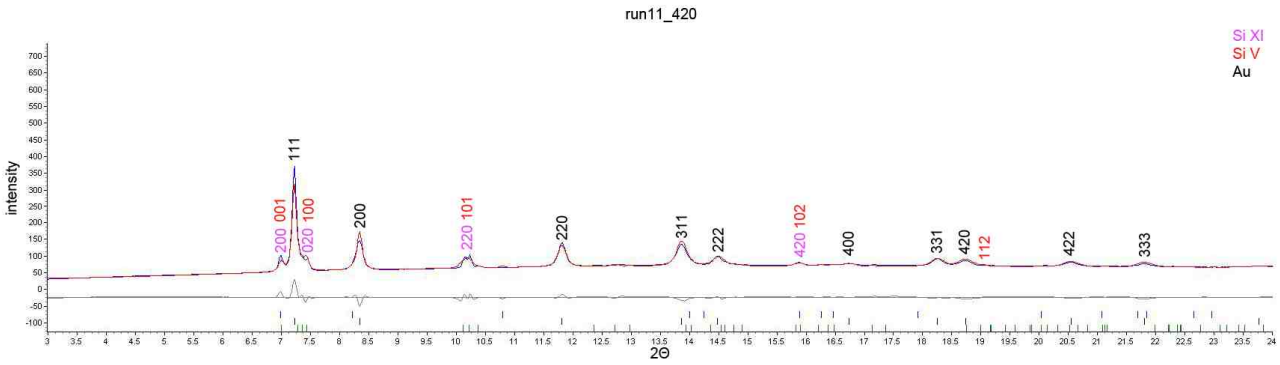

***Figure 6.24**: diffraction pattern of run11 recording 420, at a pressure of 14.52 GPa by gold Si XI and Si V are stable*

Figure 6.24 shows the refined diffraction pattern of run11 recording 420. The following values were determined using the Rietveld method:

***Table 6.22**: values of the Rietveld refinement of run11 recording 420 (GOF = 0.32)*

Phase	Lattice parameters [Å]	Quantitative portion [%]
Au	a = 3.9824878 ± 0.0008804	85
Si XI	a = 4.7449032 ± 0.0025590	14
	b = 4.5611781 ± 0.0025590	
	c = 2.5645698 ± 0.0012472	
Si V	a = 2.3368445 ± 0.0034738	1
	c = 2.3775172 ± 0.0072985	

At a pressure of 14.52 GPa by gold the phases Si XI and Si V are stable.

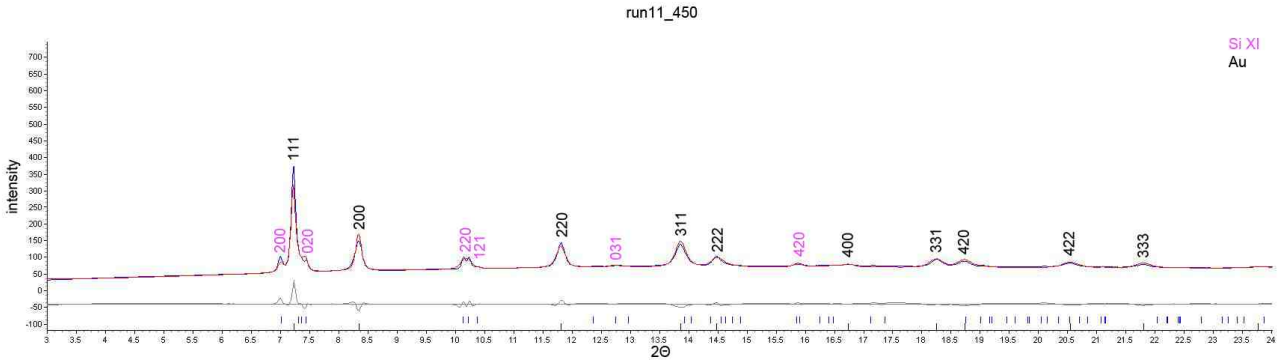

***Figure 6.25**: diffraction pattern of run11 recording 450, at a pressure of 14.50 GPa by gold Si XI is stable*

Figure 6.25 shows the refined diffraction pattern of run11 recording 450. The following values were determined using the Rietveld method:

***Table 6.23**: values of the Rietveld refinement of run11 recording 450 (GOF = 0.33)*

Phase	Lattice parameters [Å]	Quantitative portion [%]
Au	a = 3.9825306 ± 0.0007879	87
Si XI	a = 4.7419714 ± 0.0022438	13
	b = 4.5514214 ± 0.0034652	
	c = 2.5678347 ± 0.0013311	

The measurement is the last of the experiment. At a pressure of 14.50 GPa by gold the phase Si XI is stable.

The analysis of the data resulted in the following sequence of phases with increasing pressure:

$$Si\ I \rightarrow Si\ II \rightarrow Si\ XI \rightarrow Si\ V$$

Due to the high pressure gradient and the consequent low resolution no precise pressure regions can be determined. The obtained values for the pressure regions are shown in table 6.24.

***Table 6.24**: pressure ranges of the individual phases of run11*

Phase	Pressure build-up [GPa]	Pressure relief [GPa]
Si I	< 17.29	-
Si II	11.72 - 17.29	-
Si XI	11.95 - 17.29	< 14.78
SI V	> 17.29	> 14.5

Some multiphase fields with up to 3 simultaneously existing phases occur. In addition to run07 a phase transition from Si V to Si XI takes place on pressure relief, which proceeds slowly and continuous.

7 DISCUSSION

In the following, the results of the experiments are compared with the known values of the literature. The observed sequence of the Si phase is consistent with the literature (Katzke *et al.*, 2006).

$$Si\ I\ \left(Fd\overline{3}m\right) \rightarrow Si\ II\ (I4_1/amd) \rightarrow Si\ XI\ (Imma) \rightarrow Si\ V\ (P6/mmm) \rightarrow Si\ VI\ (Cmca)$$

For the two pressure gradients of 1.57 GPa/min and 44 GPa/min, the phase sequence is the same. To compare the pressure regions of the individual phases, the values of run07 are used, because of the higher resolution of pressure. The values from the literature were obtained by static experiments, allowing a comparison between static and dynamic conditions.

***Table 7.1**: pressure regions of the individual Si phases of run07 compared with the values of the literature*

Phase	Pressure build-up	Pressure relief	Literature	References

	[GPa]	[GPa]	[GPa]	
Si I	< 13.12	-	0 - 12.5	(Hu & Spain, 1984)
Si II	12.35 - 13.55	-	8.8 - 16	(McMahon & Nelmes, 1993)
Si XI	12.70 - 15.37	-	13 - 15	(McMahon & Nelmes, 1993)
SI V	15.22 - 38.67	< 36.29	14 - 35	(Olijnyk *et al.*, 1984)
Si VI	> 37.13	> 33.34	34 - 40	(Duclos *et al.*, 1990)

Table 7.1 shows that most of the pressure regions of the dynamic experiments are slightly shifted to higher pressures than the ones of the static experiments. As an exception, the phase Si II is present in a much smaller pressure region for dynamic conditions. It is transformed from Si I much later and transforms to Si XI much earlier than at static conditions. Also Si XI is the only phase that forms earlier at dynamic conditions. Maybe Si I mainly transforms directly to Si XI, with Si II as a transition phase. This could be due to the applied pressure gradient. A lack of time could cause the majority of Si I to skip the transition to Si II and directly transform to Si XI. A multi phase region with three phases is the result.

In table 7.2 the pressure regions of the phases at the different pressure gradients of run07 (1.57 GPa/min) and run11 (44 GPa/min) are listed.

***Table 7.2**: pressure regions of the phases at the different pressure gradients of run07 (1.57 GPa/min) and run11 (44 GPa/min)*

	Run07		Run11	
Phase	Pressure build-up [GPa]	Pressure relief [GPa]	Pressure build-up [GPa]	Pressure relief [GPa]
Si I	< 13.12	-	< 17.29	-
Si II	12.35 - 13.55	-	11.72 - 17.29	-
Si XI	12.70 - 15.37	-	11.95 - 17.29	< 14.78
Si V	15.22 - 38.67	< 36.29	> 17.29	> 14.5
Si VI	> 37.13	> 33.34		

Due to the higher pressure gradient of run11, the boundaries of the pressure regions are not as exact as the values of run07. Especially the upper boundaries of the pressure regions of Si I, Si II and Si XI are not recorded. It is shown that the phases Si II and Si XI occur earlier at a higher pressure gradient. A shift of the pressure regions to lower pressures at pressure relief can be noticed. Run11 shows that the phase transition of Si V to Si XI proceeds slowly and continuous. This could be due to a slow relaxation of the lattice during the displacive transformation (Katzke *et al.*, 2006).

The quantitative analysis of run07 shows that the only phase, which is not occurring alone, is Si II. This can be seen in diagram 6.3.

Using the Rietveld refinement, values of the lattice parameters of the individual phases under certain pressures were obtained. Table 7.3 shows the obtained lattice parameters in comparison with the values of the literature rounded on three decimals.

***Table 7.3**: rounded values of lattice parameter of run07 in comparison with the literature values*

Phase	$Pressure_{exp}$ [GPa]	Obtained values	$Pressure_{Lit}$ [GPa]	Literature values	References
Si I	0.66	a = 5.426	0.0001	a =5.430	(Dutta, 1962)
Si II	12.35	a = 4.615	12.5	a = 4.686	(Jamieson, 1963)
		b = 2.666		c = 2.585	
Si XI	13.12	a = 4.724	~13	a = 4.737	(McMahon & Nelmes,
		b = 4.565		b = 4.502	1993)
		c = 2.563		c = 2.550	
Si V	15.37	a = 2.552	16	a = 2.527	(Olijnyk *et al.*, 1984)
		c = 2.384		c = 2.373	
	35.20	a = 2.457	36	a = 2.463	(Duclos *et al.*, 1990)
		c = 2.321		c = 2.320	
Si VI	38.67	a = 7.989	38.4	a = 8.024	(Hanfland *et al.*, 1999)
		b = 4.784		b = 4.796	
		c = 4.762		c = 4.776	

Regarding the deviation of the observed pressures, the values of the Rietveld refinement are consistent with the literature values. For the by now little described phase Si VI, the lattice parameters shown in table 7.4 could have been refined in dependence of the pressure.

***Table 7.4**: refined lattice parameters of Si VI of run07 in dependence of the pressure*

Pressure [GPa]	a	b	c
36.29	8.013	4.799q	4.784
37.13	7.668	4.787	4.784
38.67	7.984	4.784	4.762

Outlook

For further experiments, no higher pressure gradients as the ones used should be applied to avoid further loss of resolution. To enable measurements of phases at pressure relief, the diamond anvil cell should be modified. To avoid the cell getting seized, it could be tried to smear the cylinder with oil. Another option would be honing of the cell to achieve minimum friction.

8 REFERENCES

Anderson, O. L., Isaak, D. G. & Yamamoto, S. (1989): Anharmonicity and the equation of state for gold. Journal of Applied Physics 65, 1534-1543.

Birch, F. (1952): Elasticity and constitution of the Earth's interior. Journal of Geophysical Research 57, 227-286.

Borchardt-Ott, W. (2009): Kristallographie: eine Einführung für Naturwissenschaftler. Springer Verlag, Berlin Heidelberg, 360

Duclos, S. J., Vohra, Y. K. & Ruoff, A. L. (1990): Experimental study of the crystal stability and equation of state of Si to 248 GPa. Physical Review B 41, 12021-12028.

Dutta, B. N. (1962): Lattice constants and thermal expansion of silicon up to 900 °C by X-ray method. physica status solidi 2, 984-987.

Hanfland, M., Schwarz, U., Syassen, K. & Takemura, K. (1999): Crystal Structure of the High-Pressure Phase Silicon VI. Physical Review Letters 82, 1197-1200.

Hu, J. Z., Merkle, L. D., Menoni, C. S. & Spain, I. L. (1986): Crystal data for high-pressure phases of silicon. Physical Review B 34, 4679-4684.

Hu, J. Z. & Spain, I. L. (1984): Phases of silicon at high pressure. Solid State Communications 51, 263-266.

Hull, R. (2005): Properties Of Crystalline Silicon. Institution of Engineering & Technology, London, 1016

Jamieson, J. C. (1963): Crystal Structures at High Pressures of Metallic Modifications of Silicon and Germanium. Science 139, 762-764.

Jang, J.-i., Wen, S., Lance, M. J., Anderson, I. M. & Pharr, G. M. (2003): Cracking and Phase Transformation in Silicon During Nanoindentation. MRS Proceedings 795, U8.15.

Katzke, H., Bismayer, U. & Tolédano, P. (2006): Theory of the high-pressure structural phase transitions in Si, Ge, Sn, and Pb. Physical Review B 73, 134105.

Kleber, W., Bautsch, H. J. & Bohm, J. (2010): Einführung in die Kristallographie. Oldenbourg Wissenschaftsverlag, 470

McMahon, M. I. & Nelmes, R. J. (1993): New high-pressure phase of Si. Physical Review B 47, 8337-8340.

Olijnyk, H., Sikka, S. K. & Holzapfel, W. B. (1984): Structural phase transitions in Si and Ge under pressures up to 50 GPa. Physics Letters A 103, 137-140.

Spieß, L., Teichert, G., Schwarzer, R., Behnken, H. & Genzel, C. (2009): Moderne Röntgenbeugung. Vieweg+Teubner Verlag, Wiesbaden, 564

Wille, K. (1996): Physik der Teilchenbeschleuniger und Synchrotronstrahlungsquellen.: Eine Einführung. Teubner B.G. Verlag, Leipzig, 365

Wyckoff, R. W. G. (1982): Crystal structures 1. R.E. Krieger Pub. Co., 467